Arteriosclerosis, Thrombosis, and Vascular Biology

ORIGINAL RESEARCH

ApoA-I Protects Pancreatic β-Cells From Cholesterol-Induced Mitochondrial Damage and Restores Their Ability to Secrete Insulin

Bikash Manandhar, Elvis Pandzic, Nandan Deshpande, Sing-Young Chen, Valerie Wasinger, Maaike Kockx, Elias Glaros, Kwok Leung Ong, Shane R. Thomas, Marc R. Wilkins, Renee M. Whan, Blake J. Cochran,* Kerry-Anne Rye*

BACKGROUND: High cholesterol levels in pancreatic β-cells cause oxidative stress and decrease insulin secretion. β-cells can internalize apo (apolipoprotein) A-I, which increases insulin secretion. This study asks whether internalization of apoA-I improves β-cell insulin secretion by reducing oxidative stress.

METHODS: Ins-1E cells were cholesterol-loaded by incubation with cholesterol-methyl-β-cyclodextrin. Insulin secretion in the presence of 2.8 or 25 mmol/L glucose was quantified by radioimmunoassay. Internalization of fluorescently labeled apoA-I by β-cells was monitored by flow cytometry. The effects of apoA-I internalization on β-cell gene expression were evaluated by RNA sequencing. ApoA-I-binding partners on the β-cell surface were identified by mass spectrometry. Mitochondrial oxidative stress was quantified in β-cells and isolated islets with MitoSOX and confocal microscopy.

RESULTS: An F_1-ATPase β-subunit on the β-cell surface was identified as the main apoA-I-binding partner. β-cell internalization of apoA-I was time-, concentration-, temperature-, cholesterol-, and F_1-ATPase β-subunit-dependent. β-cells with internalized apoA-I (apoA-I$^+$ cells) had higher cholesterol and cell surface F_1-ATPase β-subunit levels than β-cells without internalized apoA-I (apoA-I$^-$ cells). The internalized apoA-I colocalized with mitochondria and was associated with reduced oxidative stress and increased insulin secretion. The IF_1 (ATPase inhibitory factor 1) attenuated apoA-I internalization and increased oxidative stress in Ins-1E β-cells and isolated mouse islets. Differentially expressed genes in apoA-I$^+$ and apoA-I$^-$ Ins-1E cells were related to protein synthesis, the unfolded protein response, insulin secretion, and mitochondrial function.

CONCLUSIONS: These results establish that β-cells are functionally heterogeneous, and apoA-I restores insulin secretion in β-cells with elevated cholesterol levels by improving mitochondrial redox balance.

Key Words: cholesterol ■ insulin secretion ■ mass spectrometry ■ oxidative stress ■ temperature

Diabetes is a chronic condition that is characterized by elevated blood glucose levels due to inadequate insulin production and ineffective utilization of insulin. Diabetes is classified into 2 main types. Type 1 diabetes is an autoimmune disease in which pancreatic β-cells are selectively destroyed by autoactivated T cells, leading to reduced β-cell mass and decreased insulin secretion in response to glucose. Type 2 diabetes, which accounts for ≈90% of all diabetes, is caused by ineffective use of insulin (insulin resistance). β-cells compensate for insulin resistance by producing and secreting extra insulin. However, this ultimately causes β-cell exhaustion, progressively reduces β-cell mass, and drives progression from prediabetes to overt diabetes.

Cholesterol accumulation in β-cells also impairs insulin secretion[1–3] by reducing insulin granule exocytosis.[4,5] It also causes mitochondrial dysfunction[6] and oxidative and endoplasmic reticulum (ER) stress.[7,8] Importantly, the deleterious effect of high β-cell cholesterol levels on insulin secretion can be reversed by depleting the cells

Correspondence to: Kerry-Anne Rye, School of Biomedical Sciences, University of New S Wales, Sydney, Australia 2052. Email k.rye@unsw.edu.au
*B.J. Cochran and K.-A. Rye contributed equally as co-senior authors.
Supplemental Material is available at https://www.ahajournals.org/doi/suppl/10.1161/ATVBAHA.123.319378.
For Sources of Funding and Disclosures, see page XXX.

Arterioscler Thromb Vasc Biol is available at www.ahajournals.org/journal/atvb

Nonstandard Abbreviations and Acronyms

Apo	apolipoprotein
BCA	bicinchoninic acid
eIF2	eukaryotic initiation factor 2
ER	endoplasmic reticulum
GSIS	glucose-stimulated insulin secretion
HBSS	Hanks' Balanced Salt Solution
HDL	high-density lipoprotein
IF_1	ATPase inhibitory factor 1
KRBH	Krebs-Ringer bicarbonate-HEPES
MFI	mean fluorescence intensity
OCR	oxygen consumption rate
ROS	reactive oxygen species
UPR	unfolded protein response

of excess cholesterol with an extracellular cholesterol acceptor such as methyl-β-cyclodextrin.[2]

ApoA-I, the main apolipoprotein constituent of HDLs (high-density lipoproteins), improves glucose tolerance in high fat-fed C57BL6 mice by increasing β-cell insulin secretion and, in the case of insulin-resistant *db/db* mice, increasing glucose uptake into skeletal muscle.[9,10] ApoA-I and HDLs are the main acceptors of cholesterol that effluxes from cell membranes in a process that is dependent on the ATP-binding cassette transporters ABCA1 and ABCG1.[11] This suggests that apoA-I and HDLs may improve glucose tolerance in mice with diabetes by reducing β-cell cholesterol levels and increasing insulin secretion. However, we have found that apoA-I increases glucose-stimulated insulin secretion (GSIS) in β-cells and isolated rodent islets without altering cellular cholesterol levels.[12,13] For example, apoA-I treatment of mice with increased islet cholesterol levels and impaired insulin secretion due to conditional β-cell deletion of ABCA1 and ABCG1 markedly improves glycemic control and GSIS.[14,15] This is consistent with apoA-I improving β-cell function independent of islet cholesterol levels.

It has recently been shown that rat Ins-1E insulinoma cells internalize apoA-I by a mechanism that involves translocation of the transcription factor pancreatic and duodenal homeobox 1 to the nucleus, increased processing of proinsulin into insulin and increasing the number of insulin granules docked at the β-cell surface.[16] While this has provided some insight into how apoA-I increases insulin secretion without reducing β-cell cholesterol levels, the underlying mechanism remains unclear.

This question is addressed in the present study, which establishes that apoA-I internalization is increased in Ins-1E cells with elevated cholesterol levels and impaired GSIS and that the internalized apoA-I colocalizes with mitochondria in a process that is accompanied by reduced oxidative stress and increased insulin secretion.

Highlights

- ApoA-I (apolipoprotein A-I) is internalized by a subset of β-cells in a time-, concentration-, and temperature-dependent manner.
- ApoA-I internalization is enhanced in cholesterol-loaded β-cells.
- ApoA-I internalization by β-cells is dependent on an F_1-ATPase β-subunit.
- Internalized apoA-I colocalizes with mitochondria, reduces oxidative stress, and improves insulin secretion in cholesterol-loaded β-cells.

MATERIALS AND METHODS

Data Availability

The data that support the findings of this study are available from the corresponding author upon reasonable request.

RNA-seq datasets have been deposited into ENA (https://www.ebi.ac.uk/ena/browser/) with a primary accession number PRJEB50345. Mass spectrometry data can be accessed at https://datadryad.org/stash with the link (https://datadryad.org/stash/share/zrWZc9Mk1tVpOcGZdH9Dz6KngftJcQciplpKtC6EGos).

Cholesterol Loading of Ins-1E Cells

Ins-1E rat insulinoma cells (from Prof Claes Wollheim and Pierre Maechler, University of Geneva) were grown in RPMI 1640 medium (Thermo Fisher Scientific, Waltham, MA) containing 10% (v/v) FBS, 10 mmol/L HEPES, 2 mmol/L L-glutamine, and 1 mmol/L sodium pyruvate. Min6 mouse insulinoma cells[17] were grown in high-glucose (25 mmol/L) DMEM containing 15% (v/v) FBS, 2 mmol/L L-glutamine, and 1 mmol/L sodium pyruvate. Before experimentation, the cells were washed to remove the FBS, then incubated at 37 °C with Krebs-Ringer bicarbonate-HEPES (KRBH) buffer (10 mmol/L HEPES [pH, 7.4], 5 mmol/L $NaHCO_3$, 135 mmol/L NaCl, 3.6 mmol/L KCl, 0.5 mmol/L $MgCl_2$, 0.5 mmol/L NaH_2PO_4 and 1.5 mmol/L $CaCl_2$) containing 0.1% (w/v) BSA and 2.8 mmol/L glucose, unless stated otherwise.

Ins-1E cells were loaded with cholesterol by incubation at 37 °C for 1 hour in KRBH buffer containing cholesterol-methyl-β-cyclodextrin (final concentration, 5 mmol/L; Merck, Darmstadt, Germany).[2] After washing with ice-cold PBS, the cholesterol-loaded cells were lysed (0.2 mol/L NaOH), and the protein concentration was determined using the bicinchoninic acid (BCA) assay (Pierce BCA Protein Assay Kit, Thermo Fisher Scientific), according to the manufacturer's instructions. The samples were then partitioned into polar and nonpolar fractions using *n*-hexane and methanol (4:1 [v/v], 12.5 mL total volume). The *n*-hexane layer was removed, dried under nitrogen, and redissolved in acetonitrile:isopropanol (30:70 [v/v], 130 µL). Cell cholesterol levels were quantified by HPLC. The samples (100 µL) were injected onto a reverse-phase C18 column (Supelcosil LC-18 HPLC column, Merck) preequilibrated with acetonitrile:isopropanol (30/70 [v/v]) and eluted for 23 minutes at 1 mL/min with acetonitrile:isopropanol (30/70 [v/v]).[18]

Cholesterol was detected at 210 nm, and the concentration was determined relative to a standard curve (0–1.0 mg/mL cholesterol).

Purification of Lipid-Free apoA-I and Labeling With Alexa Fluor488

Human apoA-I (CSL Behring, King of Prussia, PA) was purified on a Q-Sepharose Fast-Flow column attached to an ÄKTA FPLC system.[19] Purity (>95%) was confirmed by SDS-PAGE and staining with Coomassie Brilliant Blue G-250 (Bio-Rad Laboratories, Hercules, CA).

ApoA-I (2–5 mg/mL) was dissolved in sodium bicarbonate (0.1 mol/L), added to AF488 (Thermo Fisher Scientific), and maintained at room temperature for 1 hour, with gentle mixing every 15 minutes. Unconjugated/free dye was removed by centrifugation at 1100*g* for 5 minutes with a resin supplied by the manufacturer. Protein concentrations and labeling efficiency were determined using a Nanodrop 1000 spectrophotometer (Thermo Fisher Scientific). AF488-labeled apoA-I was used at a final concentration of 0.1 mg/mL, unless stated otherwise.

Glucose-Stimulated Insulin Secretion

Ins-1E cells were loaded with cholesterol by incubation with cholesterol-methyl-β-cyclodextrin (5 mmol/L), washed with KRBH buffer, and incubated without or with apoA-I (final concentration, 1 mg/mL) for 2 hours under basal (2.8 mmol/L) or high (25 mmol/L) glucose conditions. The medium was then collected, and the cells were lysed (0.2 mol/L NaOH). The protein concentration of the cell lysates was measured using the BCA assay, and insulin levels were quantified using a rat insulin RIA kit (Merck).

Quantification of Insulin Levels in Ins-1E Cells Without and With Internalized apoA-I

Ins-1E cells were incubated at 37 °C for 1 hour with unlabeled apoA-I (final concentration, 0.9 mg/mL) and AF488-labeled apoA-I (0.1 mg/mL) in the absence or presence of 2.8 or 25 mmol/L glucose, then harvested and stained with propidium iodide (Merck). Live cells were sorted into those without (apoA-I^{-}) and with (apoA-I^{+}) internalized apoA-I on the basis of AF488 fluorescence (BD FACS Aria III Cell Sorter, BD Biosciences, Franklin Lakes, NJ). The sorted cells were collected into 10% (v/v) neutral-buffered formalin, fixed, and centrifuged (300*g*, 5 minutes, 4 °C). The supernatant was removed, the pellets were permeabilized (15 minutes, 4 °C), and then incubated for 30 minutes at 4 °C with an AF647-conjugated rabbit insulin antibody (Cell Signalling, Danvers, MA). Insulin levels were quantified by flow cytometry using a BD FACSCanto II flow cytometer (BD Biosciences).

Regulation of apoA-I internalization in Ins-1E Cells

The concentration-dependent internalization of apoA-I by Ins-1E cells was evaluated by incubation for 1 hour at 37 °C in KRBH buffer in the absence or presence of unlabeled and AF488-labeled apoA-I under basal (2.8 mmol/L) glucose conditions (final total apoA-I concentration, 0.1–1.0 mg/mL). AF488-labeled apoA-I was included in the incubations at one-tenth the concentration of unlabeled apoA-I.

ApoA-I internalization under basal (2.8 mmol/L) and high (25 mmol/L) glucose concentrations were evaluated by incubating Ins-1E cells at 37 °C for 1 hour in KRBH buffer in the absence or presence of unlabeled apoA-I (final concentration, 0.9 mg/mL) and AF488-labeled apoA-I (final concentration, 0.1 mg/mL).

Time-dependent apoA-I internalization was evaluated by incubating Ins-1E cells for up to 2 hours at 37 °C in KRBH buffer in the absence or presence of unlabeled apoA-I (final concentration, 0.9 mg/mL) and AF488-labeled apoA-I (final concentration, 0.1 mg/mL) under basal (2.8 mmol/L) glucose conditions. AF488 fluorescence was determined at 5, 10, 15, 30, 60, and 120 minutes.

Temperature-dependent apoA-I internalization was evaluated by incubating Ins-1E cells for 1 hour at 4 °C or 37 °C in KRBH buffer in the absence or presence of unlabeled apoA-I (final concentration, 0.9 mg/mL) and AF488-labeled apoA-I (final concentration, 0.1 mg/mL) under basal (2.8 mmol/L) glucose conditions.

The impact of cholesterol loading on apoA-I internalization was evaluated by preincubating Ins-1E cells for 1 hour in the absence or presence of cholesterol-methyl-β-cyclodextrin (final concentration, 5 mmol/L). The cholesterol-loaded cells were then incubated at 37 °C for 1 hour in the absence or presence of unlabeled apoA-I (0.9 mg/mL) and AF488-labeled apoA-I (0.1 mg/mL) under basal (2.8 mmol/L) glucose conditions.

When the incubations were complete, the cells were washed with ice-cold PBS (×2), harvested with PBS/EDTA-Na_2 (2 mmol/L), and pelleted (300*g*, 4 °C, 3 minutes). The pellets were washed twice, and cell surface AF488 fluorescence was quenched by incubation for 30 minutes at 4 °C with rabbit anti-AF488 IgG (4 µg/mL, Thermo Fisher Scientific). The difference between the signals from the cells incubated in the absence and presence of anti-AF488 IgG corresponded to apoA-I bound to the cell surface.

Live cells were identified by staining with propidium iodide (Merck). Fluorescence was measured using a FACSCanto II flow cytometer (BD Biosciences) and analyzed using FlowJo (BD Biosciences). The gating strategy is shown in Figure S4.

Identification of the F_1-ATPase β-Subunit on the Ins-1E Cell Surface

Tosylactivated Dynabeads (Thermo Fisher Scientific) were used to identify apoA-I-binding partners on the Ins-1E cell surface.[20] ApoA-I (100 µg) was dissolved in borate buffer (0.1 mol/L; pH, 9.5) containing ammonium sulfate (1.2 mol/L) and incubated at 37 °C overnight with Dynabeads (5 mg, 165 µL). The beads with bound apoA-I were collected using a magnet. Coupling efficiency was determined by measuring the unbound apoA-I concentration in the supernatant. The beads with bound apoA-I were resuspended in PBS (pH, 7.4; 250 µL) with 0.1% (w/v) BSA and incubated (5 minutes, room temperature) on a rotary shaker. The beads were collected and resuspended in PBS (250 µL) with 0.5% (w/v) BSA, then incubated for 1 hour at 37 °C to reduce nonspecific binding. The beads were collected and resuspended in PBS (250 µL) without BSA.

Ins-1E cells were seeded in a 12-well plate, washed with KRBH buffer, and maintained at 4 °C for 1 hour in KRBH

buffer/0.1% (w/v) BSA (200 µL) and Dynabeads with bound apoA-I (50 µL). The supernatant was removed, and the cells were washed with ice-cold PBS and harvested with PBS/EDTA-Na_2 (2 mmol/L). The Dynabeads were isolated with a magnet, washed with PBS (pH, 7.4)/0.1% (v/v) Tween 20, then washed with PBS (pH, 7.4). Nonspecifically bound proteins and peptides were removed from the Dynabeads by incubation overnight at room temperature with trypsin (final concentration, 0.1 mg/mL). The beads were collected using a magnet and washed (×3) with PBS. ApoA-I-binding partners were eluted with 0.15% (v/v) trifluoroacetic acid, concentrated (C18 Spin Tips, Thermo Fisher Scientific), and analyzed by LC-MS/MS.[20]

LC-MS/MS

Peptides were reconstituted in 0.1% (v/v) formic acid (10 µL) and resolved by nano-LC using an Ultimate 3000 HPLC and an autosampler (Dionex, Amsterdam, the Netherlands).[21] The sample (0.5 µL) was loaded onto a micro C18 precolumn (300 µm×5 mm; Dionex) with H_2O/CH_3CN (98/2) in 0.1% (v/v) trifluoroacetic acid at a flow rate of 10 µL/min. After washing, the precolumn was switched (Valco 10 port valve, Dionex) into line with a fritless nanocolumn (75 µm×22 cm) containing reverse-phase C18 media (particle size, 1.9 µm; pore size, 120 Å; Dr Maisch HPLC, Ammerbuch, Germany). Peptides were eluted using a linear gradient of H_2O/CH_3CN (98/2 to 64/36) in 0.1% (v/v) formic acid at 250 nL/min for 90 minutes. The QExactive (Thermo Electron, Bremen, Germany) mass spectrometer was run in DDA mode where 2000 V was applied to a low-volume union, and the column (45 °C) was positioned 0.5 cm from the heated capillary (275 °C). A survey scan at 350 to 1750 m/z was acquired in the Orbitrap (resolution, 70 000 at 200 m/z) with an accumulation target of 10^6 ions, lock mass enabled, and up to the 10 most abundant ions (AGC target set to 10^5, minimum AGC target set to 1.5×10^4) with charge states ≥+2 and ≤+6 sequentially isolated and fragmented.

Protein dataset-peak lists were generated from raw files using Mascot Daemon v2.5.1 (Matrix Science, London). All MS/MS spectra were searched against the Uniprot database (February 2021) of 563 972 sequences for protein identification with the following criteria: (1) taxon, rat; (2) allowed 1 missed cleavage; (3) variable modifications, oxidation (M), phosphorylation (S,T,Y), carbomidomethyl (C); (4) peptide tolerance, ±5 pM (5) fragment tolerance, ±0.5 Da; (6) peptide charge +2 and +3; and (7) enzyme specificity, semi-tryptic. A decoy database search was also performed. Only proteins that reached a significance threshold of $P<0.007$ (false discovery rate <1%) were recorded.

Quantification of Mitochondrial Reactive Oxygen Species

The ability of apoA-I to inhibit reactive oxygen species (ROS) formation in cholesterol-loaded Ins-1E cells was quantified by seeding cells onto a black, transparent bottom 96-well plate. When 80% confluent, the cells were incubated for 1 hour with KRBH buffer without or with 5 mmol/L cholesterol. After washing with KRBH buffer, the cells were incubated for 1 hour in the absence or presence of apoA-I (final concentration, 0.1–1 mg/mL), then incubated for 10 minutes with MitoSOX (5 µmol/L; Thermo Fisher Scientific).

Effect of apoA-I Internalization on Cholesterol-Induced Mitochondrial Oxidative Stress

Control and cholesterol-loaded Ins-1E cells were pretreated for 30 minutes with or without the protein kinase A inhibitor, H89 (final concentration, 20 µmol/L), then incubated for 1 hour in the presence or absence of apoA-I (final concentration, 1 mg/mL). ROS formation was quantified as fluorescence intensity (excitation wavelength, 510 nm; emission wavelength, 580 nm) using a Clariostar plate reader (Molecular Devices, San Jose, CA). The cells were then lysed, and the protein concentration was measured by BCA assay. Fluorescence intensity was normalized to protein concentration.

In other experiments, cholesterol-loaded Ins-1E cells with internalized apoA-I were incubated in the absence or presence of IF_1 (ATPase inhibitory factor 1). Mitochondrial oxidative stress was evaluated by incubation for 10 minutes with MitoSOX and quantified by confocal laser scanning microscopy using a Zeiss LSM880 confocal laser scanning microscope equipped with an Airyscan detector and 5% CO_2 humidified stage insert. Using super-resolution (Airyscan) mode, and a Plan-Apochromat 63×/1.4 Oil Immersion lens, images were acquired at a sampling rate of 1.1 µS/Pixel and (3800×3800) pixel arrays (pixel size, 0.04 µm). The fluorophores were excited using 405 and 514 nm lasers, which were filtered using a main bean splitter, 458/514 and main bean splitter, 405, and emission was collected in the 32-channel Airyscan GaAsP detector using BP420-475 and LP525 emission filters, respectively. Cellular MitoSOX was quantified using a custom-built script in Matlab (Natick, MA). Briefly, the images from the nuclei and MitoSOX channels were imported into Matlab, and the cells were segmented using the nuclei channel. Nuclei images were spatially filtered with Laplacian of gaussian filter with sigma equal to nuclei radii. This ensured that subnuclear structures were smoothed. Then nuclei were detected using the function pkfnd. The nucleus positions were used to perform a 2-dimensional Voronoi tessellation, and the resulting Voronoi polygons were used to identify which pixels belonged to a particular cell. This enabled the median fluorescence intensity in the MitoSOX channel to be extracted for each cell (Voronoi polygon). The data were exported into Excel and further processed by statistical analysis.

Islet Isolation

Male C57BL/6JAusb (Australian BioResources, Moss Vale, Sydney) mice were housed at the Biological Resource center, UNSW Sydney. Mice were housed in a Specific Pathogen Free facility in ventilated cages and maintained on a standard chow diet (SF00-100, Specialty Feeds, Glen Forrest, WA, Australia). Mice were euthanized by cervical dislocation, and the pancreas was distended by injecting Hanks' Balanced Salt Solution (HBSS, 2 mL with 0.23 mg/mL Liberase T-flex [Roche Diagnostics, Mannheim, Germany]) into the common bile duct (UNSW Animal Care and Ethics Committee Approval 20/53A). The tissue was digested at 37 °C for 15 minutes and quenched with HBSS/10% (v/v) FBS. Samples were filtered (500 µm netwell mesh, Merck) and then centrifuged (300*g*, 1 minute). The pellet was resuspended in HBSS/10% (v/v) FBS (20 mL), shaken vigorously, and centrifuged. The pellet was washed twice with HBBS/FBS, then resuspended in Ficoll-Paque PLUS (20 mL, GE Healthcare Life Sciences, Chicago, IL). HBSS/10%

(v/v) FBS (10 mL) was layered on top of the suspension, then centrifuged (1370*g*, 22 minutes, 4 °C), and the supernatant was filtered (100 µm cell strainer, BD Biosciences). Islets that were trapped on the mesh were washed with HBSS/10% (v/v) FBS, then washed with prewarmed islet media (RPMI, 10% [v/v] FBS, 10 mmol/L HEPES, 2 mmol/L L-glutamine, 1 mmol/L sodium pyruvate). The mesh was then inverted onto a 60-mm petri dish, and the islets were eluted with 10 mL of RPMI 1640 medium, 10% (v/v) FBS, 10 mmol/L HEPES, 2 mmol/L L-glutamine, and 1 mmol/L sodium pyruvate.

Dependence of apoA-I Internalization on Cell Surface F_1-ATPase β-Subunit in Ins-1E Cells and Primary Islets

Cell surface F_1-ATPase β-subunit levels were quantified by incubating Ins-1E cells for 1 hour at 4 °C with a mouse IgG_1 kappa antibody (isotype control [1:100]; final concentration, 10 µg/mL) or a mouse anti-F_1-ATPase β-subunit antibody (3D5 clone [1:50]; final concentration, 10 µg/mL, Abcam, Cambridge, United Kingdom). The cells were then incubated for 30 minutes at 4 °C with AF647-conjugated goat anti-mouse IgG (1:500, Thermo Fisher Scientific). Cholesterol levels were determined by incubation for 30 minutes at 4 °C with filipin (50 µg/mL). Live cells were identified with propidium iodide. Mean fluorescence intensity (MFI) was determined using a BD LSRFortessa X-20 flow cytometer (BD Biosciences).

Cell surface F_1-ATPase β-subunit in Ins-1E cells was blocked by preincubation (37 °C, 15 minutes) with IF_1 (final concentration, 10 µg/mL; Creative BioMart, Shirley, NY) in KRBH buffer/0.1% (w/v) BSA (pH, 6.4). The cells were then incubated (30 minutes, 37 °C) with AF488-labeled apoA-I (final concentration, 0.1 mg/mL), washed with ice-cold PBS, harvested, and incubated (30 minutes, 4 °C) with rabbit anti-AF488 IgG (4 µg/mL, Thermo Fisher Scientific). AF488 fluorescence was quantified by flow cytometry (BD FACSCanto II flow cytometer, BD Biosciences).

Handpicked islets were incubated overnight (37 °C, 5% CO_2) in a humidified incubator (35-mm glass bottom fluorodish; Cellvis, Mountain View, CA). The medium was removed, the islets were washed with KRBH buffer, then incubated (37 °C, 15 minutes) in KRBH buffer/0.1% (w/v) BSA (pH 6.4) with or without IF_1 (final concentration, 10 µg/mL). AF488-labeled apoA-I (0.1 mg/mL) was added, and the cells were incubated for 1 hour at 37 °C. Hoechst 33342 (Thermo Fisher Scientific, 1:200 dilution [v/v] of a 10 mg/mL solution) was added, and the islets were incubated for 10 minutes. The islets were washed with KRBH buffer, fixed (15 minutes, room temperature, 10% [v/v] formalin), permeabilized, then incubated overnight at 4 °C with AF647-conjugated rabbit insulin antibody (1:100, Cell signalling). After washing, ProLong Diamond Antifade Mountant (Thermo Fisher Scientific) was added dropwise, and the samples were maintained at 4 °C until imaged (Zeiss LSM 880 confocal microscope with Airyscan, Carl Zeiss Microscopy, Jena, Germany).

Confocal Microscopy of Isolated Islets

Three-dimensional stacks of islets incubated with IF_1 were acquired in Airyscan resolution enhanced mode with an undersampled step size of 4 µm and optical section thickness of 0.64 µm. Rather than using Nyquist sampling for full 3-dimensional representation, Z-stacks were undersampled in the *z* axis at 4 µm intervals to avoid photo-bleaching and ensure robust comparative analysis. The images were acquired in a 2628×2628 pixel array with 0.04 µm per pixel (30.3 seconds per frame) and a pixel dwell time of 1.6 µs using a C-Apochromat 40×/1.1 water immersion lens. The fluorophores were excited with 488 (AF488), 405 (Hoechst 33342), and 647 (AF647) nm lasers and collected in the 32-channel Airyscan GaAsP detector using the BP500-545, BP420-480, and LP655 emission filters, respectively. The AF488 fluorescence images were analyzed with custom-built scripts in MATLAB R2021a, and the median fluorescence intensity of AF488 across all z-stacks of individual islets was calculated.

Briefly, imaged z-stacks were loaded in Matlab with a user-defined lower-intensity threshold to exclude voxels outside of the islets, and an upper-intensity threshold to exclude bright clusters of apoA-I that accumulated but did not play a functional role. With the threshold in place, a 3-dimensional binary mask with relevant voxels equal to 1, and 0 for nonrelevant voxels, fluorescence intensity from the 488-nm channel (apoA-I) was extracted for all the voxels in the mask, and the median fluorescence intensity per islet was calculated. This was repeated for all islets and all conditions, and the data were exported into an Excel spreadsheet for statistical analysis.

Regulation of Cholesterol-Induced Mitochondrial Oxidative Stress by Internalized apoA-I

Ins-1E cells were seeded onto a 35-mm glass bottom fluorodish (Cellvis) and incubated (37 °C, 1 hour) with KRBH buffer in the absence or presence of 5 mmol/L cholesterol. The cells were washed with KRBH buffer (×2), incubated with KRBH buffer/0.1% (w/v) BSA (pH, 6.4) without or with IF_1 (final concentration, 10 µg/mL), incubated with apoA-I (final concentration, 1 mg/mL) for 1 hour, then incubated for 10 minutes with MitoSOX (1 µmol/L, Thermo Fisher Scientific) and Hoechst 33342 (1:200 [v/v]). The samples were washed with KRBH buffer, and mitochondrial oxidative stress was quantified by confocal laser scanning microscopy.

Localization of internalized apoA-I in the Ins-1E cells was determined by incubation for 1 hour at 37 °C with unlabeled apoA-I (final concentration, 0.9 mg/mL) and AF488-labeled apoA-I (final concentration, 0.1 mg/mL), then incubation at 37 °C for 10 minutes with MitoTracker Red CM-H2XRos (Thermo Fisher Scientific). The cells were washed with PBS, fixed with 10% (v/v) formalin, washed again with PBS, then imaged with a Zeiss LSM880 microscope in super-resolution (Airyscan) mode. Mander coefficient for percentage of AF488 overlap with MitoTracker was calculated by comparing the AF488 and MitoTracker channels for the apoA-I group or the MitoTracker channel flipped 90° clockwise for the control group, using the Just Another Colocalization Plugin in FIJI software (National Institutes of Health, Bethesda, MD).

RNA Isolation and Sequencing

Ins-1E cells were incubated for 1 hour with unlabeled apoA-I (final concentration, 0.9 mg/mL) and AF488-labeled apoA-I (0.1 mg/mL) in the presence of 2.8 mmol/L glucose, then harvested.

Live cells were identified by staining with 7-amino-actinomycin D (7-AAD; Thermo Fisher Scientific), then sorted into those without (apoA-I$^-$), and those with internalized apoA-I (apoA-I$^+$) on the basis of AF488 fluorescence using a BD FACSMelody cell sorter (BD Biosciences). Total RNA was collected and purified using an RNeasy mini kit (Qiagen, Hilden, Germany) as per the manufacturer's protocol. Total RNA was quantified with a Nanodrop 1000 spectrophotometer (Thermo Fisher Scientific). RNA was analyzed for quality and integrity using an Agilent 2100 Bioanalyzer (Agilent Technologies, Santa Clara, CA) and sequenced. Libraries were prepared from 500 ng of total RNA/sample using TruSeq Stranded mRNA-seq prep. Each library was single-read sequenced (1×75 bp) using NextSeq 500 High Output flowcell (60 million reads per sample).

Bioinformatic Analysis

RNA-seq reads were first assessed for quality using the FastQC tool (v0.11.8) (www.bioinformatics.babraham.ac.uk/projects/fastqc/). The tool Salmon was used for quantifying transcript abundance from RNA-seq reads.[22] A rat transcriptome that contained the super-set of all transcripts coding sequences resulting from Ensembl gene predictions (Rnor_6.0.101) was downloaded and converted into a Salmon index file (ftp://ftp.ensembl.org/pub/release-101/fasta/rattus_norvegicus/cds/). This index file was used as a reference file for the mapping and quantification step. Transcript-level quantifications were converted to gene-level quantifications for downstream differential expression analysis.

Differentially expressed genes across all of the conditions were identified using the Bioconductor package edgeR v3.28.0 in the R programming environment.[23] Read counts were normalized using the between-lane normalization of EDASeq with upper quartile normalization.[24] The RUV R package was used to remove unwanted variation caused by batch effects using empirical control genes.[25] Differentially expressed genes identified with a false discovery rate of <0.1 were considered to be significantly upregulated or downregulated. Ingenuity Pathway Analysis software (Qiagen) was used to identify canonical pathways associated with the differentially expressed genes in apoA-I$^-$ and apoA-I$^+$ Ins-1E cells.

Western Blotting

Ins-1E cells were incubated (1 hour, 37 °C) in absence or presence of apoA-I (final concentration, 0.1 or 1 mg/mL). The cells were washed with ice-cold PBS (×2), then lysed with RIPA buffer. Mitochondrial and cytoplasmic lysates were prepared using a cell fractionation kit (Abcam). Protein concentration was measured by BCA assay. Cell, mitochondrial, and cytoplasmic proteins (10 µg) were resolved by SDS-PAGE (Bolt, 4%–12%, Bis-Tris Plus, Thermo Fisher Scientific) and then transferred to a PVDF membrane. The membrane was blocked with 5% (w/v) skim milk in TBS/0.5% (v/v) Tween 20 (TBS-T) and incubated overnight with goat anti-apoA-I (1:200, Merck), mouse anti-cytochrome c oxidase subunit 1 (MT-CO1, 1:250; Santa Cruz, Dallas, TX) or mouse anti-β-actin (1:1000, Merck) antibodies. The membrane was then washed with TBS-T, incubated (1 hour) with rabbit anti-goat IgG (Bio-Rad, Hercules, CA) or goat anti-mouse IgG (1:2000, Bio-Rad), and developed using ECL (GE Healthcare). The proteins were visualized and imaged using ImageQuant LAS 4000 (GE Healthcare).

Regulation of Insulin Secretion by mitoTEMPO

Ins-1E cells were incubated with 5 mmol/L cholesterol for 1 hour at 37 °C, then incubated for a further 1 hour in the absence or presence of mitoTEMPO (final concentration, 1 mmol/L, Sigma-Aldrich, St Louis, MO) under basal (2.8 mmol/L) glucose conditions. The supernatant was collected, and the cells were lysed with RIPA buffer before protein quantification with the BCA assay. The insulin concentration in the supernatant was determined with an ultra-sensitive rat insulin ELISA kit (Crystal Chem, Elk Grove Village, IL) according to the manufacturer's instructions. The results were normalized to cell protein.

Effect of apoA-I on Oxygen Consumption Rate in Ins-1E Cells

Oxygen consumption rate (OCR) was determined using a Seahorse XF Cell Mito Stress Test kit (Agilent, Santa Clara, CA) and a Seahorse XFe96 analyzer (Agilent) according to the manufacturer's instructions with slight modifications. Briefly, Ins-1E cells were seeded (5×10^4 cells/well) in a XF96 cell culture microplate (Agilent). When 80% confluent, the cells were incubated for 1 hour at 37 °C in KRBH buffer, then incubated for a further 1 hour in KRBH buffer with or without apoA-I (final concentration, 0.1 or 1 mg/mL) under basal (2.8 mmol/L) glucose conditions. The cells were then washed before addition of Seahorse assay media (200 µL, Seahorse XF RPMI medium; pH, 7.4, Agilent), supplemented with 1 mmol/L pyruvate, 2 mmol/L glutamine, and 2.8 mmol/L glucose. The microplate was then incubated at 37 °C for 1 hour in a non-CO_2 incubator under humidified conditions. The medium was replaced with a fresh prewarmed assay medium and transferred to the Seahorse XFe96 analyser with a precalibrated XFe96 sensor cartridge for OCR measurements. The Seahorse protocol was designed to measure OCR at repeated cycles of 3 minutes of mixing and 3 minutes of measurement for a total of 13 measurements. Oligomycin (final concentration/well, 2.5 µmol/L) was added after the fourth measurement, carbonyl cyanide *p*-trifluoro-methoxyphenyl hydrazone (FCCP; final concentration in well, 1 µmol/L) was added after the seventh measurement and rotenone/antimycin A mix (final concentration in well, 0.5 µmol/L) was added after the tenth measurement. At the end of the experiment, the cells were lysed with RIPA buffer, and the total protein was quantified by the BCA assay. The data were processed (Wave Desktop software, Version 2.6, Agilent) and normalized to cell protein. Basal respiration was calculated as the difference between the last OCR rate before oligomycin injection and the average of 3 measurements of the OCR rate after rotenone/antimycin A mix injection.

Effect of Cholesterol Loading on Ins-1E Cell Viability

Ins-1E cells were loaded with 0, 1, 5, or 10 mmol/L cholesterol by incubation for 1 hour at 37 °C in the absence or presence of cholesterol-methyl-β-cyclodextrin. A live and dead cell assay kit (Abcam) was used to identify the dead cells by fluorescence microscopy and flow cytometry. Fluorescence images were acquired with EVOS M5000 microscope (Thermo Fisher Scientific) and analyzed qualitatively. The percentage live cells were quantified using a BD FACSCanto II flow analyzer (BD Biosciences), and cell viability was expressed as percentage control.

Effect of Cholesterol Loading and apoA-I on Ins-1E Cell Protein Level

Ins-1E cells were seeded (2×10^4 cells/well) on a transparent, clear-bottom 96-well plate and incubated at 37 °C. After 48 hours, the cells were incubated for 1 hour at 37 °C with or without cholesterol-methyl-β-cyclodextrin (final cholesterol concentration, 5 mmol/L). The cells were washed with KRBH buffer (×2), then incubated for 1 hour at 37 °C in the absence or presence of apoA-I (final concentration, 1 mg/mL) under basal (2.8 mmol/L) glucose conditions. The cells were washed once with ice-cold PBS, lysed with ice-cold RIPA buffer (60 µL), and then incubated for 30 minutes on ice. The protein concentration was determined by BCA assay at 562 nm with a microplate reader (VERSAmax, Bio-strategy, Melbourne).

Statistical Analyses

Results are presented as the mean±SEM of at least 3 independent biological experiments. Statistically significant differences between data sets were identified by 1-sample Student *t* test (*P* values denoted by #), unpaired, 2-tailed Student *t* test (*P* values denoted by *), and 1-way ANOVA with Tukey multiple comparison test (*P* values denoted by *) where appropriate. GraphPad Prism (Version 9.4, San Diego, CA) was used for all analyses with $P<0.05$ considered as statistically significant.

RESULTS

ApoA-I Increases GSIS in Noncholesterol-Loaded and Cholesterol-Loaded Ins-1E Cells

Incubation of Ins-1E cells with cholesterol-methyl-β-cyclodextrin in the absence of apoA-I increased intracellular cholesterol levels from 24±1.7 to 41±2.4 µg/mg protein (Figure 1A; $P<0.001$ versus control), and to 38±2.2 µg/mg protein in the presence of apoA-I (Figure 1A; $P<0.01$ versus control).

When cholesterol-loaded Ins-1E cells were incubated under basal (2.8 mmol/L glucose) conditions, insulin secretion decreased by 44±4.3%, compared with Ins-1E cells with normal cholesterol levels (Figure 1B; $P<0.01$). In the presence of apoA-I, insulin secretion increased by 95±8.4% compared with cholesterol-loaded cells incubated without apoA-I (Figure 1B; $P<0.01$).

The same pattern was observed under high (25 mmol/L) glucose conditions, where GSIS in cholesterol-loaded Ins-1E cells decreased by 60±9.7% compared with control Ins-1E cells (Figure 1C; $P<0.01$). Incubation with apoA-I restored GSIS in the cholesterol-loaded Ins-1E cells back to that of cells with normal cholesterol levels (Figure 1C; $P<0.05$ versus cholesterol-loaded cells without apoA-I).

Incubation of noncholesterol-loaded Ins-1E cells with apoA-I under basal (Figure 1B; 2.8 mmol/L) and high (Figure 1C; 25 mmol/L) glucose conditions increased insulin secretion by 80±22% and 350±116%, respectively, relative to cholesterol-loaded Ins-1E cells incubated in the presence of apoA-I (Figure 1B and 1C; $P<0.05$ for both). Incubation with apoA-I and cholesterol loading does not affect Ins-1E protein levels (Figure S1) or cell viability (Figure S2).

Ins-1E Cells Selectively Internalize apoA-I in a Time-, Temperature-, Concentration-, and Cholesterol-Dependent Manner

Although the ability of apoA-I to increase GSIS in Ins-1E cells with normal cholesterol levels has been reported to depend on its internalization,[16] it is not known whether

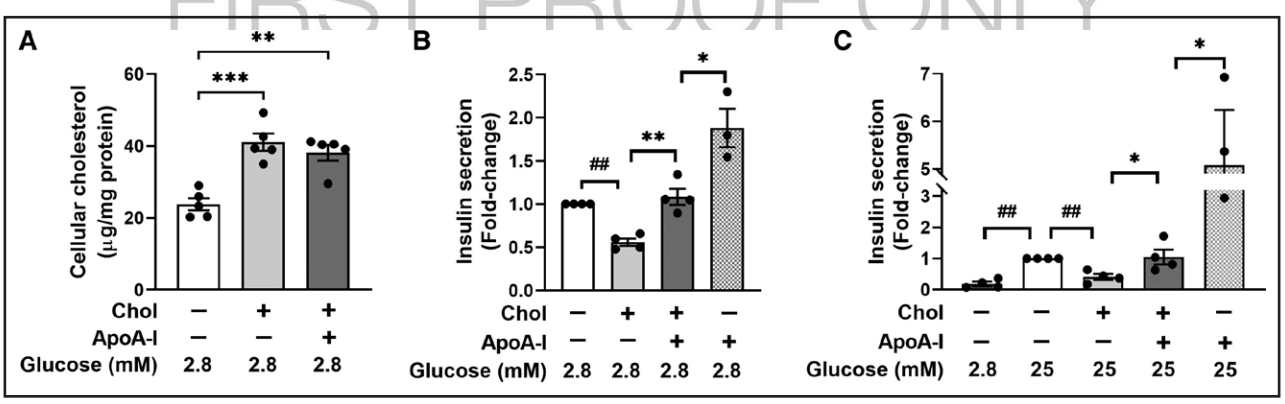

Figure 1. ApoA-I (apolipoprotein A-I) increases glucose-stimulated insulin secretion (GSIS) in noncholesterol-loaded and cholesterol-loaded Ins-1E cells.
Ins-1E cells were incubated for 1 hour at 37 °C in the absence or presence of cholesterol-β-methyl cyclodextrin (5 mmol/L cholesterol), washed with PBS then incubated for 2 hours without or with apoA-I (final concentration, 1 mg/mL). **A**, Cells were incubated at 37 °C for 1 hour in the presence and absence of cholesterol-β-methyl cyclodextrin. Cholesterol levels were measured by HPLC and normalized to cell protein concentration. Noncholesterol-loaded and cholesterol-loaded cells were incubated in the presence and absence of apoA-I under basal (2.8 mmol/L; **B**) and high (25 mmol/L; **C**) glucose conditions. Insulin levels in the medium were quantified by RIA, normalized to cell protein concentration, and expressed as fold-change relative to control. The values represent mean±SEM of 4 to 5 independent biological experiments, with 3 to 4 technical replicate samples for each independent experiment. **A** was analyzed by 1-way ANOVA and Tukey multiple comparison test. **B** and **C** were analyzed by 1-sample *t* test or unpaired 2-tailed *t* test, as appropriate. *$P<0.05$, **$P<0.01$, ***$P<0.0001$, ##$P<0.01$.

this is also the case for cholesterol-loaded Ins-1E cells. This was addressed by incubating Ins-1E cells with AF488-labeled apoA-I. To ensure that only intracellular fluorescence was quantified, cell surface AF488 fluorescence was quenched at the end of the incubation with an anti-AF488 antibody.

When Ins-1E cells with normal cholesterol levels were incubated with AF488-labeled apoA-I in the presence of 0, 2.8, and 25 mmol/L glucose, fluorescence increased by 502±77%, 420±87%, and 374±93%, respectively (Figure 2A; $P<0.05$ for all). This indicates that apoA-I internalization is independent of glucose concentration.

However, apoA-I was not internalized uniformly. For the incubations in the absence of glucose, Ins-1E cells without (apoA-I$^-$ cells) and with internalized apoA-I (apoA-I$^+$ cells) were identified (Figure 2B). This was also observed when Min6 cells were incubated with apoA-I (Figure S3A). In the absence of glucose, AF488 fluorescence in the apoA-I$^+$ cells was 25-fold higher than in the control cells (3114±561 versus 121±19 MFI) and 8-fold higher in the apoA-I$^-$ cells (3114±561 versus 347±27 MFI; Figure 2C; $P<0.01$ for both). Fluorescence in the apoA-I$^+$ Ins-1E cells was also increased relative to control and apoA-I$^-$ cells following incubation under basal (2.8 mmol/L; Figure 2D) and high (25 mmol/L; Figure 2E) glucose conditions ($P<0.001$ for all).

In the presence of 0, 2.8, and 25 mmol/L glucose, the Ins-1E cells with internalized apoA-I comprised 43±3.6%, 39±5.1%, and 35±6.2% of the total cells, respectively (Figure 2F). The AF488 MFI in these cells did not change, regardless of the glucose concentration (Figure S5A). The percentage of apoA-I$^+$ cells increased linearly to 31±7.4% during the first 30 minutes of incubation and 50±3.2% of the apoA-I was internalized by 2 hours (Figure 2G).

ApoA-I internalization, as reflected by AF488 MFI, increased linearly up to 2 hours (Figure 2H), and was concentration-dependent (Figure 2I; Figure S5B). It was also temperature-dependent, with 6.9±3.8% of the Ins-1E cells containing internalized apoA-I after 1 hour at 4 °C compared with 45±8.0% for cells that were incubated for 1 hour at 37 °C (Figure 2J; $P<0.05$). This translates into a 200±6.0% increase in apoA-I internalization at 37 °C relative to 4 °C (Figure S5C; $P<0.001$). ApoA-I internalization was also increased in cholesterol-loaded Ins-1E cells relative to cells that were not cholesterol-loaded (Figure 2K; $P<0.05$). However, cholesterol loading had no impact on the proportion of cells that internalized apoA-I (47.9±5.6% and 34.9±1.9% for control versus cholesterol-loaded cells, respectively; Figure S5D).

ApoA-I Binds to an F_1-ATPase β-Subunit on the Ins-1E Cell Surface

To identify proteins on the Ins-1E cell surface on which apoA-I internalization is dependent, purified apoA-I was coupled to Dynabeads and added to Ins-1E cells at 4 °C, a temperature at which apoA-I internalization is minimal (Figure 2J; Figure S5C). The Ins-1E cell surface proteins that bound to Dynabead-coupled apoA-I were identified by mass spectrometry. The β-subunit of F_1-ATPase, a mitochondrial protein that is localized on the surface of several cell types, including Ins-1E cells was identified as a main apoA-I-binding partner (Table S1).[26–29] The presence of this protein on the Ins-1E cell surface was confirmed by flow cytometry using 3D5, an F_1-ATPase β-subunit-specific antibody (Figure 3A and 3B; $P<0.05$ for isotype control versus 3D5).

ApoA-I Internalization in Ins-1E Cells Correlates With Cell Surface F_1-ATPase β-Subunit, Cholesterol, and Insulin Levels

To determine how the cell surface F_1-ATPase β-subunit regulates apoA-I internalization, unmodified and cholesterol-loaded Ins-1E cells were preincubated with AF488-labeled apoA-I, then incubated with the 3D5 antibody. Cellular unesterified cholesterol levels were quantified with filipin.

Cholesterol loading increased filipin fluorescence by 42±7.2% in control Ins-1E cells (Figure 3C, open bars; $P<0.01$) and by 36±5.3% in the cells that were incubated with apoA-I (Figure 3C, closed bars; $P<0.0001$). Incubation with apoA-I did not affect filipin fluorescence, irrespective of whether the cells were cholesterol-loaded (Figure 3C). This is consistent with Figure 1A, where cholesterol levels in cholesterol-loaded Ins-1E cells were not altered by incubation with apoA-I. Neither cholesterol loading nor incubation with apoA-I altered Ins-1E cell surface F_1-ATPase β-subunit levels (Figure 3D).

As only a proportion of the Ins-1E cells internalized apoA-I (Figure 2B through 2E), the impact of this heterogeneity on cell surface F_1-ATPase β-subunit levels was evaluated. Unmodified and cholesterol-loaded Ins-1E cells were incubated with apoA-I and sorted into apoA-I$^+$ and apoA-I$^-$ cells. Cholesterol and cell surface F_1-ATPase β-subunit levels were quantified with filipin and 3D5, respectively. In the absence of cholesterol loading, filipin fluorescence in the apoA-I$^+$ Ins-1E cells was 132±13% higher than in apoA-I$^-$ Ins-1E cells (Figure 3E; $P<0.01$). Filipin fluorescence in the cholesterol-loaded apoA-I$^+$ Ins-1E cells was 109±10% higher than cholesterol-loaded apoA-I$^-$ Ins-1E cells (Figure 3E; $P<0.0001$). Filipin fluorescence in the cholesterol-loaded apoA-I$^+$ Ins-1E cells was 19±7.0% higher than in apoA-I$^+$ Ins-1E cells that were not loaded with cholesterol (Figure 3E, closed bars; $P<0.05$).

In the absence of cholesterol loading, cell surface F_1-ATPase β-subunit levels in apoA-I$^+$ Ins-1E cells were 172±33% higher than in apoA-I$^-$ Ins-1E cells (Figure 3F; $P<0.05$). Cell surface F_1-ATPase β-subunit levels were

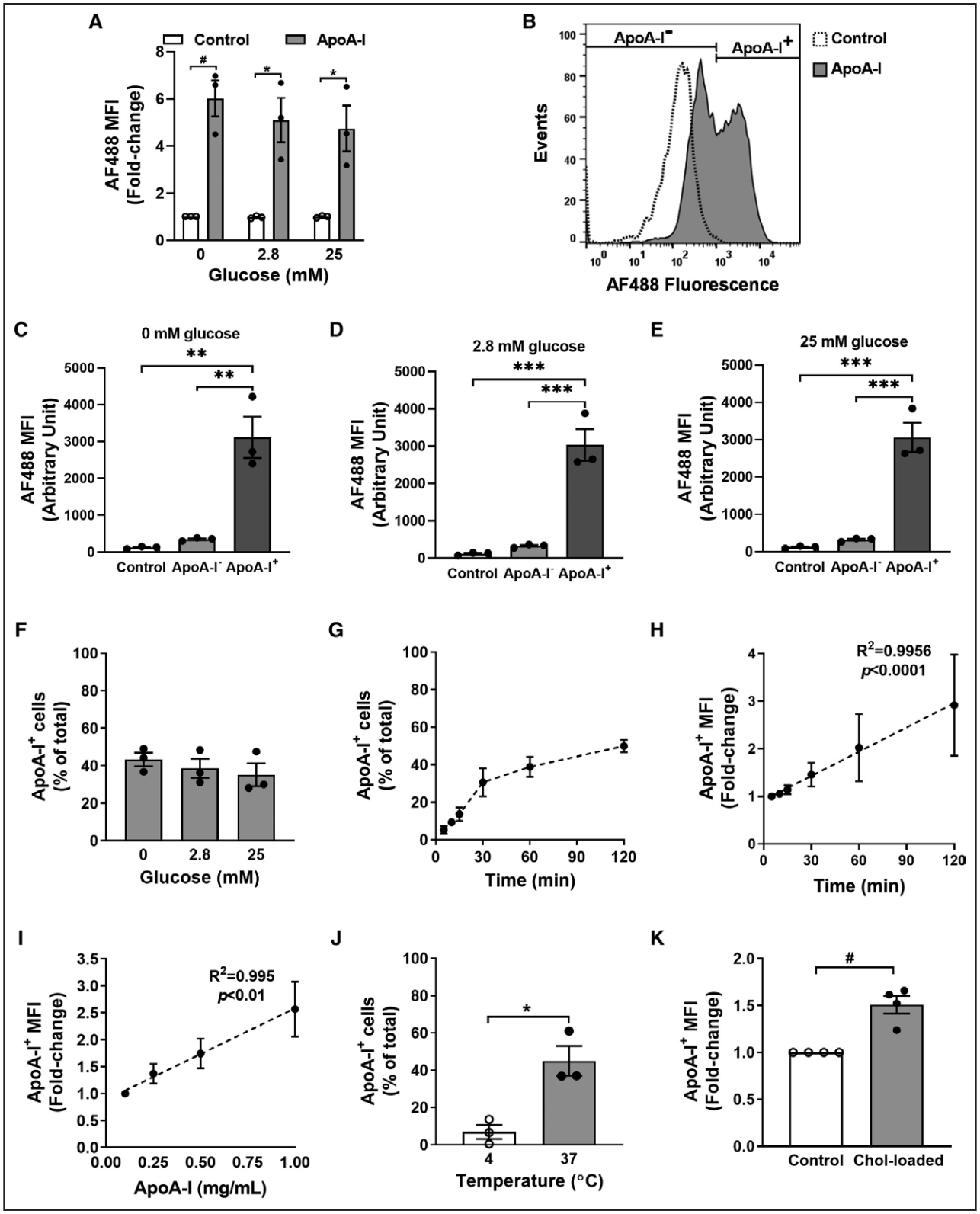

Figure 2. ApoA-I (apolipoprotein A-I) is internalized by a subset of Ins-1E cells in a time-, temperature-, and cholesterol-dependent manner.

Ins-1E cells were incubated for 1 hour at 37 °C in the absence or presence of unlabeled apoA-I (final concentration, 0.9 mg/mL), AF488-labeled apoA-I (final concentration, 0.1 mg/mL) and 0, 2.8, or 25 mmol/L glucose. AF488 internalization was quantified by flow cytometry. **A** shows mean fluorescence intensity (MFI) of AF488 in cells incubated in the absence (open bars) or presence (closed bars) of 0, 2.8, and 25 mmol/L glucose. Based on AF488 fluorescence relative to control, Ins-1E cells that were incubated with AF488-labeled apoA-I in the absence of glucose were gated as apoA-I⁻ cells or apoA-I⁺ cells (**B**). MFI of AF488 in the control, apoA-I⁻ and apoA-I⁺ subsets of Ins-1E (*Continued*)

also significantly higher in apoA-I$^+$ Min6 cells (P<0.0001; Figure S3B). Cell surface F_1-ATPase β-subunit levels in cholesterol-loaded cells were 142±9% higher in apoA-I$^+$ Ins-1E cells than in apoA-I$^-$ Ins-1E cells (Figure 3F; P<0.01).

Insulin levels were also quantified in Ins-1E cells following incubation with apoA-I in the absence or presence of 2.8 or 25 mmol/L glucose. Insulin levels in apoA-I$^+$ cells were 62±11% (ns), 68±6.6% (P<0.05), and 67±4.7% (P<0.01) lower than in apoA-I$^-$ Ins-1E cells in the absence or presence of 2.8 and 25 mmol/L glucose (Figure 4A and 4B). Insulin levels were also significantly lower in apoA-I$^+$ Min6 cells than in apoA-I$^-$ Min6 cells under basal glucose (2.8 mmol/L) conditions (P<0.0001; Figure S3C).

Differential Gene Expression in apoA-I$^-$ and apoA-I$^+$ Ins-1E Cells

Having established that intracellular cholesterol (Figure 3E), cell surface F_1-ATPase β-subunit (Figure 3F), and total insulin levels (Figure 4A and 4B) differ significantly in apoA-I$^-$ and apoA-I$^+$ Ins-1E cells, we next asked whether these differences are also reflected in altered gene expression. ApoA-I$^-$ and apoA-I$^+$ Ins-1E cells were subjected to RNA-seq and canonical pathways with differentially regulated genes were identified by Ingenuity Pathway Analysis. Principal component analysis showed that gene expression in the apoA-I$^-$ and apoA-I$^+$ Ins-1E cells clustered separately (Figure 4C), which is consistent with different gene expression profiles in these cell subsets. Out of a total of 6808 genes, 459 were differentially expressed in apoA-I$^-$ and apoA-I$^+$ Ins-1E cells, with 258 genes being upregulated, and 201 genes being downregulated in apoA-I$^+$ cells relative to apoA-I$^-$ Ins-1E cells (FDR≤0.1; Figure 4D). After excluding 121 unidentified differentially expressed genes, the remaining 338 genes were analyzed by Ingenuity Pathway Analysis. The top 5 pathways that were significantly altered were eIF2 (eukaryotic initiation factor 2) signaling (−log[P value]: 8.69), unfolded protein response (UPR; −log[P value]: 4.97), insulin secretion signaling (−log[P value]: 3.85]), mitochondrial dysfunction (−log[P value]: 2.61), and oxidative phosphorylation (−log[P value]: 2.42; Figure 4E; Table S2). Seventeen genes involved in eIF2 signaling and 7 genes involved in the UPR were upregulated in apoA-I$^+$ Ins-1E cells relative to apoA-I$^-$ Ins-1E cells (Table S2).

Increased mRNA levels of chaperones such as calnexin (*Canx*), calreticulin (*Calr*), UBX domain protein 4 (*Ubxn4*), and X-box binding protein 1 (*Xbp1*) that target proteins for correct folding or degradation in the UPR suggest that the increased ER stress in apoA-I$^+$ Ins-1E cells may be caused by increased protein synthesis and defective protein folding (Table S2). Genes associated with insulin signaling and secretion that were upregulated in apoA-I$^+$ Ins-1E cells included *Ins1* and *Ins2*. This contrasts with the result in Figure 4B, which shows that apoA-I$^+$ Ins-1E cells have lower insulin levels than apoA-I$^-$ Ins-1E cells. Only 4 genes associated with insulin secretion were downregulated in apoA-I$^+$ Ins-1E cells compared with apoA-I$^-$ Ins-1E cells. These downregulated genes included translocon subunit gamma (*Sec61g*), which translocates proteins, including preproinsulin, from the cytosol to the ER and ryanodine receptor 1 (*Ryr1*), which regulates β-cell ER Ca^{2+} homeostasis (Table S2).

Other differentially expressed genes were associated with oxidative phosphorylation and mitochondrial dysfunction (Table S2). Mitochondrial genes encoding for NADH dehydrogenase (respiratory complex I), including NADH-ubiquinone oxidoreductase chain 5 protein (*Mt-Nd5*) and NADH-ubiquinone oxidoreductase chain 6 protein (*Mt-Nd6*), were downregulated in apoA-I$^+$ Ins-1E cells compared with apoA-I$^-$ Ins-1E cells, while other genes such as NADH dehydrogenase (ubiquinone) 1 beta subcomplex subunit 2, mitochondrial (*Ndufb2*) and NADH dehydrogenase (ubiquinone) 1 beta subcomplex subunit 8, mitochondrial (*Ndufb8*) were upregulated. Similarly, mitochondrial genes including cytochrome c oxidase subunit 2 (*Mt-Co2*), a subunit of respiratory complex IV, and the ATP synthase F_0 subunit 6 (*Mt-Atp6*) were downregulated in apoA-I$^+$ Ins-1E cells compared with apoA-I$^-$ Ins-1E cells, while the mitochondrial ATP synthase F_1 subunit delta (*Atp5f1d*) was upregulated.

Internalized apoA-I Localizes to Mitochondria in Ins-1E Cells

Having established that several genes involved in mitochondrial redox function are differentially regulated in apoA-I$^+$ Ins-1E cells, we next asked whether internalized apoA-I localizes to the mitochondria.

When Ins-1E cells were incubated with AF488-labeled apoA-I and MitoTracker, then subjected to confocal microscopy, a high degree of colocalization of

Figure 2 Continued. cells incubated with 0 (**C**), 2.8 (**D**), and 25 (**E**) mM glucose are shown. The percentage of Ins-1E cells that internalized AF488-labeled apoA-I in absence or presence of 2.8 and 25 mmol/L glucose is shown in **F**. The percentage of Ins-1E cells that internalized AF488-labeled apoA-I and the AF488 MFI over 120 minutes are shown in **G** and **H**, respectively. **I**, The AF488 MFI of apoA-I$^+$ Ins-1E cells following incubation for 1 hour with unlabeled apoA-I (0.09–0.9 mg/mL) and AF488-labeled apoA-I (0.01–0.1 mg/mL). **J**, The percentage of apoA-I$^+$ Ins-1E cells after incubation for 1 hour at 4 °C and 37 °C. **K**, The MFI of apoA-I$^+$ cells in control and cholesterol-loaded cells. Values in **A** and **C** through **K** represent the mean±SEM of 3 to 4 independent biological experiments, with 10 000 events per acquisition. Data in **A**, **J**, and **K** were analyzed by 1-sample t test or unpaired, 2-tailed t test, as appropriate. **C** through **F** were analyzed by 1-way ANOVA and Tukey multiple comparison tests. Simple linear regression was used to calculate the slopes in **H** and **I**. *P<0.05, **P<0.01, ***P<0.001, #P<0.05.

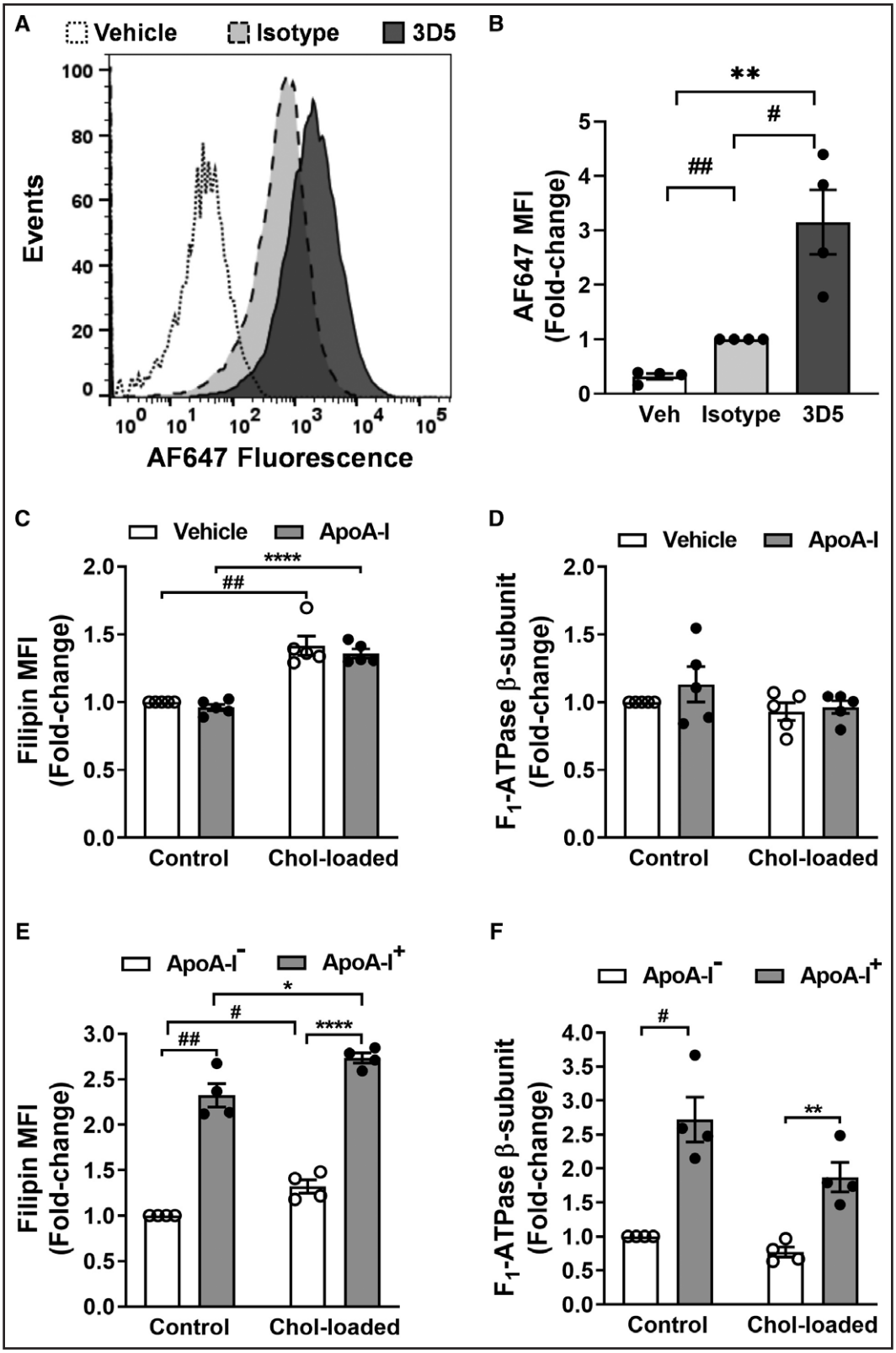

Figure 3. Cholesterol loading increases apoA-I (apolipoprotein A-I) internalization in Ins-1E cells without altering cell surface F_1-ATPase β-subunit levels.

Ins-1E cells were incubated in Krebs-Ringer bicarbonate-HEPES (KRBH) buffer for 1 hour, harvested, fixed with 10% (v/v) formalin, and incubated for 1 hour at 4 °C with PBS (vehicle), isotype IgG control (1:50, 10 µg/mL), or the 3D5 anti-F_1-ATPase β-subunit antibody (1:100, 10 µg/mL). The cells were washed with PBS, then incubated for 30 minutes at 4 °C with an AF647-labeled secondary antibody (1:500). Representative flow cytometry histograms (**A**) and the mean fluorescence intensity (MFI; **B**) of AF647 are shown. **C** through **F**, (*Continued*)

internalized AF488-labeled apoA-I with MitoTracker was observed (Figure 5A through 5C). The Mander coefficient of colocalization was 0.7±0.1 (Figure 5D; $P<0.01$).

Colocalization of internalized apoA-I with mitochondria was confirmed by Western blotting of whole cells and mitochondrial and cytoplasmic subfractions (Figure 5E). ApoA-I was not detected in the whole-cell lysates or mitochondrial or cytoplasmic subfractions in cells that were not incubated with apoA-I (Figure 5E). Following incubation with apoA-I, whole-cell lysates and the mitochondrial fraction were apoA-I-enriched relative to the cytoplasmic fraction (Figure 5E). MT-CO1, a mitochondrial-enriched protein, and β-actin (loading control) are also shown (Figure 5E). The different migration of β-actin in the mitochondrial and cytoplasmic fractions likely reflects the use of a proprietary buffer for cellular subfractionation, while RIPA buffer was used for whole-cell lysates.

ApoA-I Reduces Mitochondrial ROS Levels in Cholesterol-Loaded Ins-1E Cells

Elevated cholesterol levels increase mitochondrial ROS production and reduce mitochondrial antioxidant enzymes, leading to GSIS suppression.[30,31] Conversely, mitochondrial-targeted antioxidants reduce oxidative stress and improve β-cell insulin secretion.[32] To determine if the apoA-I that colocalized with mitochondria in cholesterol-loaded apoA-I+ Ins-1E cells reduces mitochondrial ROS generation, unmodified and cholesterol-loaded Ins-1E cells were incubated in the absence or presence of apoA-I. Mitochondrial ROS levels were quantified with MitoSOX.

Cholesterol loading increased mitochondrial ROS formation in the Ins-1E cells by 27±7.6% compared with Ins-1E cells with normal cholesterol levels (Figure 5F; $P<0.05$). Inclusion of apoA-I in the incubations decreased mitochondrial ROS formation by 51±5.2% (Figure 5F; $P<0.001$) in a concentration-dependent manner (Figure 5G; $P<0.01$). Pretreatment of the cells with the protein kinase A inhibitor, H89, which reduces apoA-I-mediated GSIS,[13] blocked the antioxidant action of apoA-I (Figure S6A) but did not affect apoA-I internalization (Figure S6B). ApoA-I had no effect on mitochondrial oxygen consumption rate (OCR) or basal respiration in Ins-1E cells (Figure S7A and S7B). This indicates that apoA-I does not affect mitochondrial respiration.

Reducing ROS Production With the Mitochondrial Antioxidant mitoTEMPO Increases Insulin Secretion in Cholesterol-Loaded Ins-1E Cells

To establish whether decreased mitochondrial ROS generation was associated with increased insulin secretion, cholesterol-loaded Ins-1E cells were incubated in the absence or presence of mitoTEMPO, a mitochondrial-targeted antioxidant. The results showed that cholesterol loading decreased insulin secretion in Ins-1E cells by 54±6.5% (Figure S8; $P<0.0001$). Incubation of the cholesterol-loaded Ins-1E cells with mitoTEMPO increased insulin secretion by 43±7.7% (Figure S8; $P<0.01$) compared with cholesterol-loaded Ins-1E cells incubated in the absence of mitoTEMPO.

ApoA-I Decreases Mitochondrial ROS Levels in Cholesterol-Loaded Ins-1E Cells and Isolated Islets in a Cell Surface F_1-ATPase β-Subunit-Dependent Manner

We next tested whether inhibiting apoA-I binding to cell surface F_1-ATPase β-subunit with IF_1 also blocks its internalization.[29,33] IF_1 inhibited AF488-labeled apoA-I internalization in Ins-1E cells by 31±2.3% (Figure 6A and 6B; $P<0.01$). This suggests that apoA-I internalization is dependent, at least in part, on binding to the F_1-ATPase β-subunit.

This result was recapitulated in incubations of isolated mouse islets with AF488-labeled apoA-I and IF_1. Relative to islets incubated with apoA-I only, the MFI of internalized AF488-labeled apoA-I decreased by 44±9.0% in the presence of IF_1 (Figure 6C and 6D; $P<0.0001$). The presence of β-cells in the islets was confirmed by staining for insulin (Figure 6C). Merging of the AF488-labeled apoA-I and insulin images showed colocalization of apoA-I within insulin-positive cells in the islets after incubation with apoA-I. This colocalization was reduced by incubation in the presence of IF_1 (Figure 6C).

In agreement with the MitoSOX data in Figure 5E and 5F, confocal microscopy further established that the median fluorescence intensity of MitoSOX in cholesterol-loaded Ins-1E cells was increased by 148±1.7% relative to control (Figure 6E and 6F; $P<0.0001$). In the presence of apoA-I, MitoSOX fluorescence intensity and mitochondrial ROS generation in cholesterol-loaded Ins-1E cells decreased by 49±1.2%

Figure 3 Continued. Ins-1E cells were loaded with 5 mmol/L cholesterol as described in the legend to Figure 1 then incubated for 1 hour in the absence or presence of unlabeled apoA-I (0.9 mg/mL) and AF488-labeled apoA-I (0.1 mg/mL). The cells were harvested, fixed with 10% (v/v) formalin, and incubated for 1 hour at 4 °C with 3D5 (1:100, 10 µg/mL). After washing with PBS, the cells were incubated for 30 minutes at 4 °C with an AF647-labeled secondary antibody (1:500), then incubated for 30 minutes at 4 °C with filipin. MFI of filipin (**C**) and cell surface F_1-ATPase β-subunit (**D**) in control and apoA-I treated cells are shown. MFI of filipin (**E**) and cell surface F_1-ATPase β-subunit (**F**) in apoA-I− cells (open bars) and apoA-I+ cells (closed bars) are shown. The values in **B** through **F** represent mean±SEM of 4 to 5 independent biological experiments, with 10 000 events per acquisition. Data in **B** through **F** were analyzed via 1-sample *t* test or unpaired, 2-tailed *t* test, as appropriate. *$P<0.05$, **$P<0.01$, ****$P<0.0001$, #$P<0.05$, ##$P<0.01$.

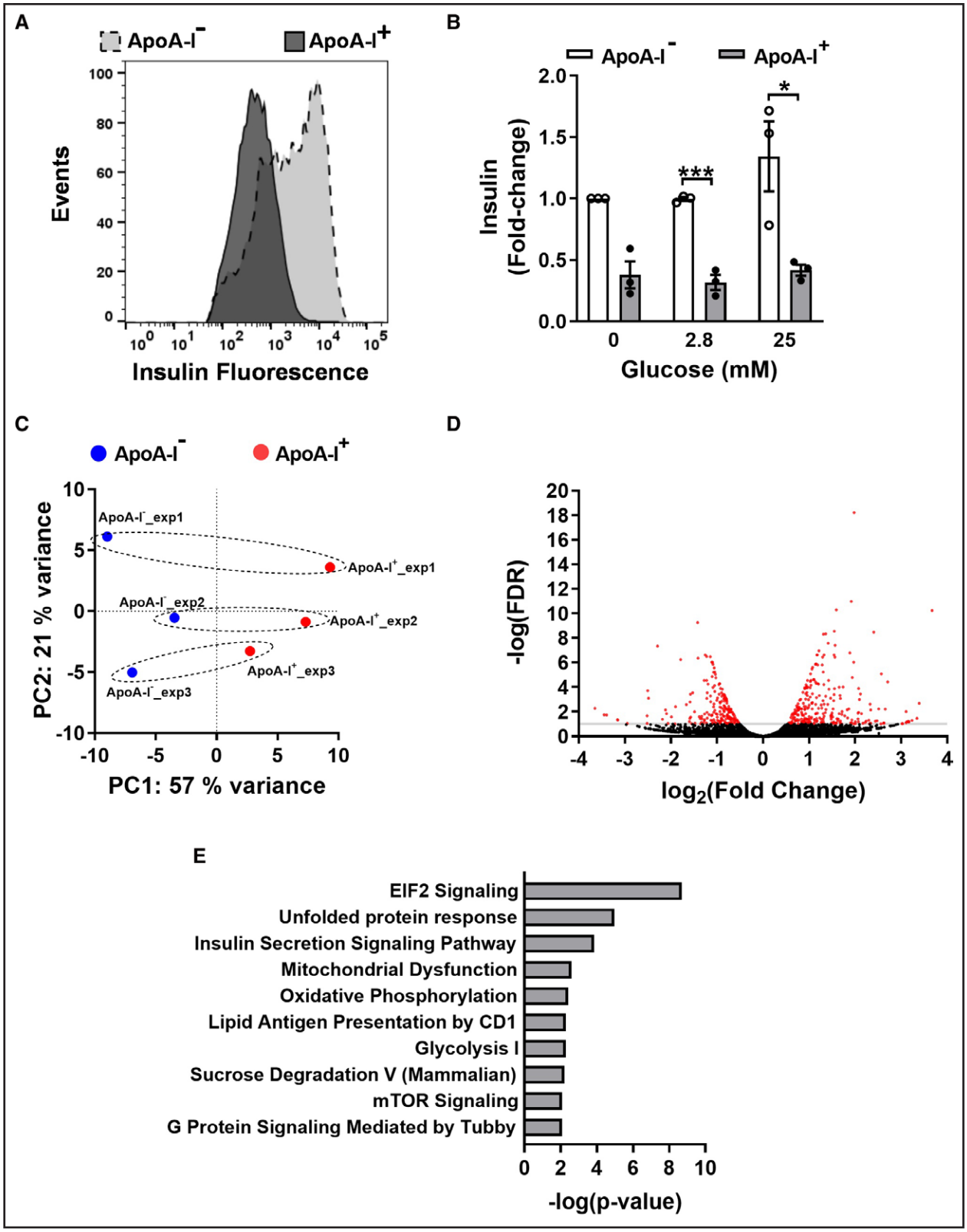

Figure 4. Ins-1E cells that internalize apoA-I (apolipoprotein A-I) have reduced insulin levels and differentially regulated genes. Ins-1E cells were incubated at 37 °C for 1 hour with unlabeled apoA-I (0.9 mg/mL) and AF488-labeled apoA-I (0.1 mg/mL) in the absence or presence of glucose (2.8 and 25 mmol/L) and then sorted into apoA-I⁻ cells and apoA-I⁺ cells based on AF488 fluorescence. The sorted cells were fixed, permeabilized, and incubated for 30 minutes at 4 °C with an AF647-conjugated anti-insulin antibody. A representative histogram (**A**) and the mean fluorescence intensity (MFI; **B**) of insulin in the apoA-I⁻ and apoA-I⁺ Ins-1E cells are shown. **C**, Two-dimensional principal component analysis plots for apoA-I⁺ and apoA-I⁻ Ins-1E cells from 3 independent experiments. Differentially expressed (*Continued*)

(Figure 6F; $P<0.0001$). Inclusion of IF_1 in the incubation increased mitochondrial ROS generation by 92±2.7% compared with cholesterol-loaded cells incubated only with apoA-I (Figure 6F; $P<0.0001$). Collectively, these results indicate that apoA-I internalization is likely responsible for the observed improvement in mitochondrial function.

DISCUSSION

Elevated cholesterol levels are associated with reduced β-cell insulin secretion.[1–3] This has been attributed, at least in part, to oxidative stress as a result of mitochondrial cholesterol accumulation[6,7] and mitochondrial dysfunction.[30] Depleting cholesterol from cholesterol-loaded β-cells restores insulin secretion.[2] ApoA-I also increases insulin secretion in Ins-1E and MIN6 cells, but this is independent of cellular cholesterol levels.[12–14] The present study establishes that apoA-I increases insulin secretion in cholesterol-loaded Ins-1E cells and isolated mouse islets by binding to an ectopic, cell surface mitochondrial F1-ATPase β-subunit. This facilitates the internalization of apoA-I into the cell where it colocalizes with mitochondria and decreases oxidative stress, leading to increased insulin secretion.

It has been reported previously that apoA-I internalization is necessary for increasing insulin secretion in Ins-1E cells and isolated islets with normal cholesterol levels.[16] The present study established that this is also the case for Ins-1E cells with elevated cholesterol levels. We also found that apoA-I is internalized in a subset of cholesterol-loaded Ins-1E cells with reduced insulin levels. This is consistent with other reports of the insulin secretory capacity of Ins-1E cells being variable.[34]

The present study further establishes that apoA-I internalization by Ins-1E cells and isolated islets is dependent on binding to an ectopic, cell surface F_1-ATPase β-subunit. The F_1-ATPase β-subunit is part of the mitochondrial ATP-producing machinery that includes F_0F_1 ATPase (ATP synthase or complex V). The F_1-ATPase β-subunit is mainly localized on the inner mitochondrial membrane of eukaryotic cells, but it has also been reported on the surface of Ins-1E cells, endothelial cells, and hepatocytes.[26,35] Although the binding of apoA-I to the F_1-ATPase β-subunit has been reported to mediate HDL (high-density lipoprotein) uptake in hepatocytes and vascular endothelial cells via the purinergic receptor P2Y13,[29,36] this receptor was not identified as an HDL-binding partner by mass spectrometry and therefore seems not to have a role in apoA-I internalization in Ins-1E cells.

The binding of apoA-I to the F_1-ATPase β-subunit on the hepatocyte surface increases ATP hydrolysis and stimulates a purinergic G protein-coupled P2Y receptor signaling cascade that culminates in HDL endocytosis. It also increases survival and proliferation of vascular endothelial cells and drives the transcytosis of apoA-I and HDLs across vascular endothelial cells into the subendothelial space.[33,36,37] How the F_1-ATPase β-subunit translocates from mitochondria to the cell surface is unclear but seems to depend on brefeldin A in neural cells.[38] Whether this is also the case in other cell types is not known. Mitochondria-derived vesicles can also transport proteins from the mitochondria toward peroxisomes and lysosomes, and possibly toward the plasma membrane.[39,40] Whether these mechanisms are responsible for the translocation of the F_1-ATPase β-subunit from mitochondria to the Ins-1E cell surface remains to be determined.

One of the most important observations from the present study is the preferential internalization of apoA-I by Ins-1E cells with elevated cholesterol levels. This is consistent with what has been reported for apoA-I internalization in cerebral microvascular endothelial cells via an endocytic process that is inhibited when cell cholesterol levels are reduced with methyl β-cyclodextrin.[41] However, in contrast to a previous study where cholesterol loading increased translocation of the F_1-ATPase β-subunit to the surface of vascular endothelial cells,[42] we found that cholesterol loading had no effect on cell surface F_1-ATPase β-subunit levels in Ins-1E cells.

Heterogeneity in the insulin secretory capacity of mouse β-cells and human islets has been documented previously.[43–45] This is consistent with the elevated cholesterol and cell surface F_1-ATPase β-subunit levels, lower insulin levels, and functional heterogeneity of the Ins-1E cells with internalized apoA-I in the present study. Additional evidence of functional heterogeneity of Ins-1E cells comes from the observation that genes involved in ER stress and the UPR are upregulated in apoA-I$^+$ Ins-1E cells. ER stress also impairs the ABCA1-mediated efflux of cholesterol from hepatocytes.[46] This may explain why cholesterol levels were increased in the apoA-I$^+$ Ins-1E cells. However, it is unclear if this is a cause or consequence of ER stress.

Reduced expression of *Sec61g* and *Ryr1* that respectively encode for the transport proteins Sec61 subunit gamma and ryanodine receptor 1 in the ER membrane further suggest that ER-associated oxidative folding of insulin and conversion of preproinsulin to proinsulin is decreased in apoA-I$^+$ Ins-1E cells.[47–49] This may explain why apoA-I$^+$ Ins-1E cells have lower insulin levels than apoA-I$^-$ Ins-1E cells despite having increased *Ins1* and *Ins2* expression (Figure 4A and 4B). It is also consistent with decreased expression of mitochondrial genes

Figure 4 Continued. genes (red) with an FDR of ≤0.1 are shown (**D**). The top 10 canonical pathways based on differential gene expression in apoA-I$^+$ Ins-1E cells relative to apoA-I$^-$ Ins-1E cells were identified by ingenuity pathway analysis (**E**). The values in **B** represent the mean±SEM of 3 independent biological experiments, with 10 000 events per acquisition. Data in **B** were analyzed via 1-sample *t* test or unpaired 2-tailed *t* test, as appropriate. *$P<0.05$, ***$P<0.001$. EIF2 indicates eukaryotic initiation factor 2.

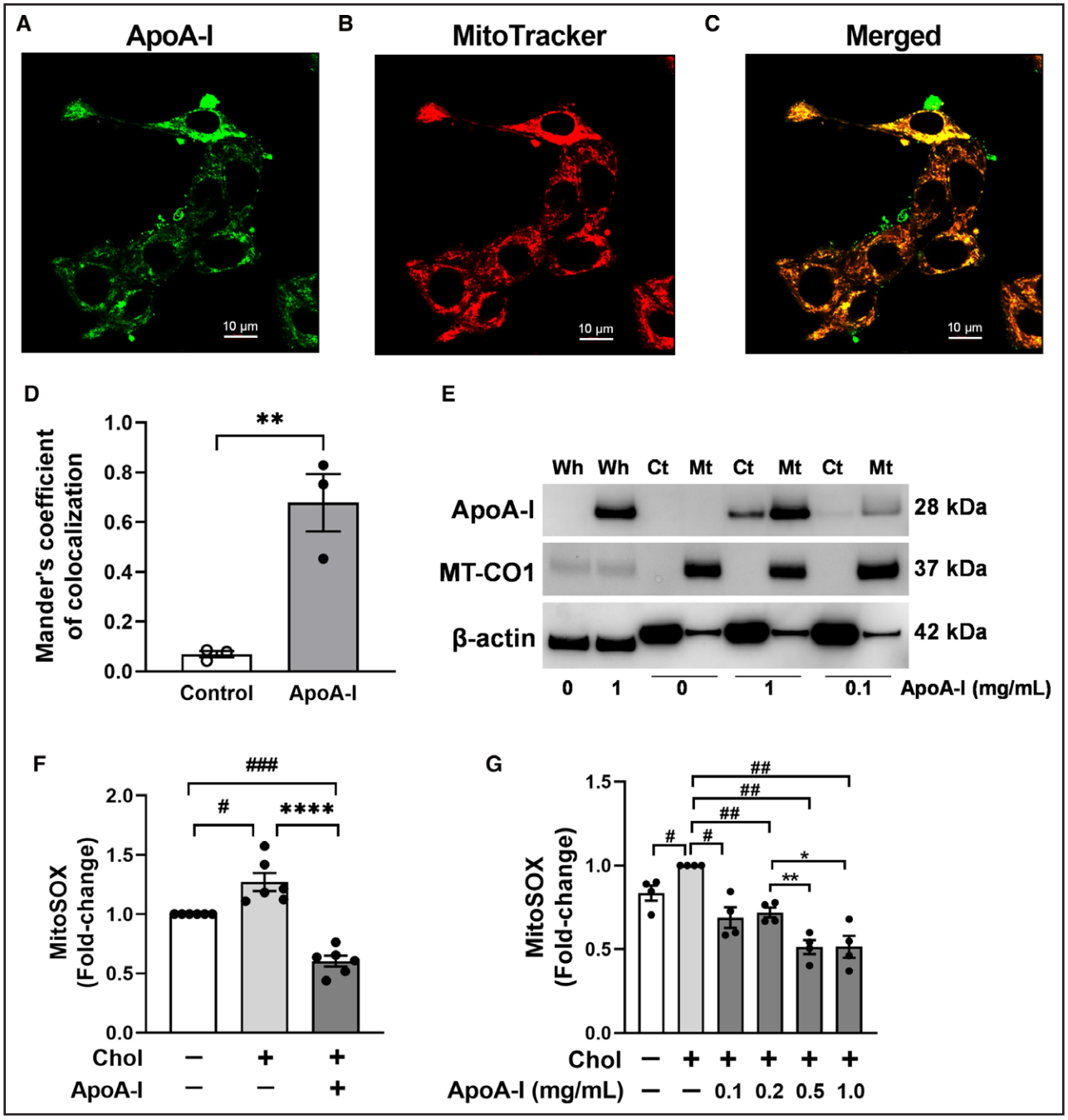

Figure 5. ApoA-I (apolipoprotein A-I) colocalizes with mitochondria and reduces cholesterol-induced reactive oxygen species (ROS) generation in Ins-1E cells.

Ins-1E cells were incubated at 37 °C for 1 hour with unlabeled apoA-I (0.9 mg/mL) and AF488-labeled apoA-I (0.1 mg/mL), then incubated for 10 minutes with MitoTracker. The cells were washed, fixed, and AF488 fluorescence was evaluated using a Zeiss LSM880 microscope with super-resolution (Airyscan) mode. Fluorescence images of apoA-I (**A**) and MitoTracker (**B**) and a merged image (**C**) are shown. **D**, The Mander coefficient of AF488 overlap with MitoTracker. This result is the mean±SEM of 3 independent biological experiments with 6 to 9 images/experiment. **E**, A representative Western blot (from 3 independent experiments) of apoA-I, MT-CO1, and β-actin in whole cell lysates (Wh), and the cytoplasmic (Ct) and mitochondrial (Mt) fractions from Ins-1E cells incubated at 37 °C for 1 hour in absence or presence of apoA-I (0.1 or 1 mg/mL). **F**, MitoSOX fluorescence in control and cholesterol-loaded Ins-1E cells after 1 hour of incubation at 37 °C with Krebs-Ringer bicarbonate-HEPES buffer or apoA-I (1 mg/mL). **G**, MitoSOX fluorescence in cholesterol-loaded Ins-1E cells, following incubation at 37 °C for 1 hour in the absence or presence of apoA-I (0.1–1.0 mg/mL). MitoSOX fluorescence was normalized to cell protein. The values in **F** and **G** represent the mean±SEM of 4 to 6 independent biological experiments, with 6 replicate samples for each independent experiment. Data in **D**, **F**, and **G** were analyzed via 1-sample *t* test or unpaired, 2-tailed *t* test, as appropriate. *P<0.05, **P<0.01, ****P<0.0001, #P<0.05, ##P<0.01, ###P<0.001.

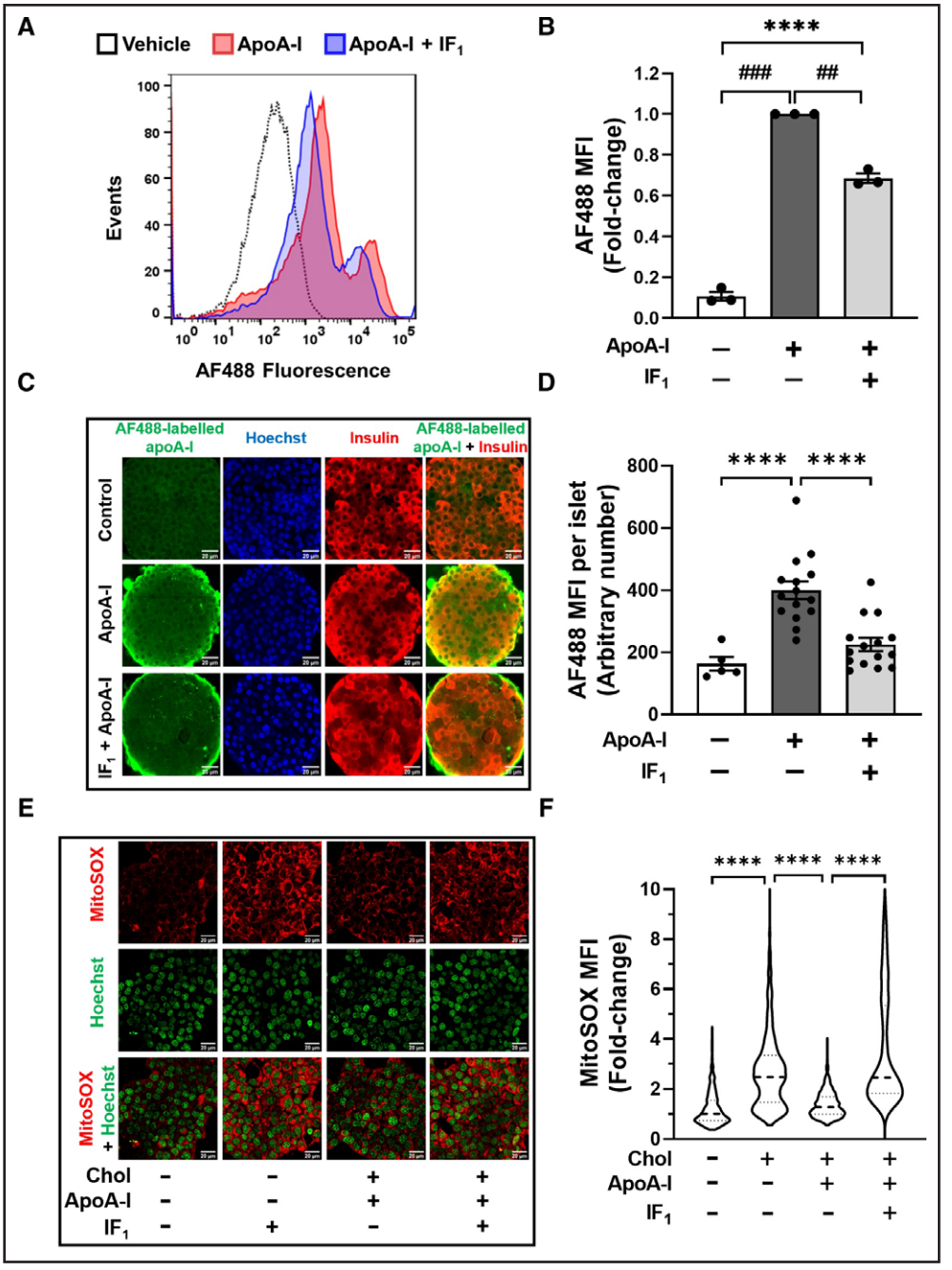

Figure 6. IF_1 (ATPase inhibitory factor 1) inhibits apoA-I (apolipoprotein A-I) internalization and promotes reactive oxygen species (ROS) generation in cholesterol-loaded Ins-1E cells and isolated islets.

Ins-1E cell or islets isolated from male C57BL/6JAusb mice were preincubated at 37 °C for 15 minutes in Krebs-Ringer bicarbonate-HEPES (KRBH) buffer without or with IF_1 (10 µg/mL), then incubated at 37 °C for 30 minutes with KRBH buffer, 0.1% (w/v) BSA (vehicle), or AF488-labeled apoA-I (0.1 mg/mL) in the presence or absence of IF_1 (10 µg/mL). Representative histograms (**A**) and mean fluorescence intensity (MFI; **B**) of AF488 are shown. **C** and **D**, Isolated islets that were preincubated at 37 °C for 15 minutes in KRBH buffer (pH, 6.4) with or without IF_1 (10 µg/mL), incubated at 37 °C for 2 hours with KRBH buffer, 0.1% (w/v) BSA (vehicle) or AF488-labeled apoA-I (0.1 mg/mL), then incubated at 37 °C with Hoechst 33342 (1:200 [v/v]) for 10 minutes. When the incubations were complete, the islets were washed with KRBH buffer, fixed, permeabilized, and incubated overnight at 4 °C with an AF647-labeled anti-insulin antibody (1:100). Representative confocal images (**C**) and MFI of AF488 in individual islets (**D**) are shown. **E** and **F**, Control and cholesterol-loaded cells were incubated for 15 minutes in KRBH buffer (0.1% BSA [v/v]; pH, 6.4) without or with IF_1 (final concentration, 10 µg/mL). The cells were further incubated for 1 hour in the presence or absence of apoA-I (final concentration, 1 mg/mL), followed by incubation with MitoSOX (1 µmol/L) and Hoechst 33342 (1:200 dilution [v/v]) for 10 minutes. Representative confocal images (**E**) and MFI of MitoSOX (**F**) are shown. **B**, The mean±SEM of 3 to 4 independent biological experiments. **D**, Mean±SEM of 5 to 15 islets from each of 3 mice. **F**, The median value of 1185 to 1474 cells from 3 independent biological experiments. Data in **B** were analyzed via a 1-sample *t* test or unpaired, 2-tailed *t* test, as appropriate. Data in **D** and **F** were analyzed via 1-way ANOVA, followed by Tukey multiple comparison test. $^{****}P<0.0001$, $^{\#\#}P<0.01$, $^{\#\#\#}P<0.001$.

involved in oxidative phosphorylation and function that produce ATP and drive insulin secretion in apoA-I$^+$ Ins-1E cells (Table S2).

Heterogeneity in UPR activation and ER oxidative stress have been reported in isolated human islets.[50] This may be caused by β-cells cycling from periods of (1 high insulin synthesis and low UPR to (2) ER stress, increased UPR, and low insulin synthesis to (3) resolved ER stress and low insulin synthesis.[51] It is possible that the Ins-1E cell heterogeneity in the present study reflects the transitioning of Ins-1E cells across similar dynamic states, rather than stable subtypes. It is also possible that the Ins-1E heterogeneity in the present study reflects hub Ins-1E cells that internalize apoA-I and are highly metabolic, transcriptionally immature, and have low insulin levels.[52] The internalization of apoA-I by hubs could modulate function and alter the insulin secretory capacity of cells that do not internalize apoA-I. β-cells that are defined as hubs underpin the responses of islets to changes in glucose levels, making them essential for GSIS.[45] Moreover, as the viability of β-cell hubs is diminished by glucotoxicity and glucolipotoxicity, it follows that these cells may play a fundamentally important role in diabetes prevention.[45]

The current results indicate that cholesterol enrichment exacerbates ER and oxidative stress and reduces insulin secretory capacity in Ins-1E cells. The antioxidant functions of apoA-I have been well characterized[53] and have been attributed to reduced levels of ROS and increased expression of antioxidant enzymes including superoxide dismutase and glutathione peroxidase.[54] The present study indicates that apoA-I internalization may increase the insulin secretory capacity of Ins-1E cells with elevated cholesterol levels by inhibiting mitochondrial ROS production and restoring mitochondrial redox balance. Further studies are needed to determine whether comparable β-cell subpopulations are present in human islets and whether they are potential targets for pharmacological inhibition of oxidation.

A limitation of the present study is that relative to its level in normal human plasma, the concentration of lipid-free apoA-I used in the GSIS experiments could be considered as supraphysiological. However, it is important to note that lipid-free and lipid-associated apoA-I (as a constituent of reconstituted HDLs) both increase GSIS equally effectively.[12] This is consistent with the capacity of apoA-I to increase insulin secretion being independent of whether it is lipid-free or lipid-associated. It therefore follows the apoA-I concentration to which the Ins-1E cells were exposed in the GSIS experiments is physiologically relevant. Another limitation of the study is that only islets from male C57BL6J mice were used to determine whether IF_1 reduces colocalization of internalized apoA-I with insulin-positive cells (Figure 6C). Male mice were used because they have a higher β-cell mass and secrete more insulin in response to glucose than female mice and were therefore expected to display an enhanced response to IF_1.[55]

In conclusion, this study establishes that apoA-I restores insulin secretion in β-cells with disrupted cholesterol homeostasis by binding to an ectopic F1-ATPase β-subunit, internalizing into the cells and localizing to mitochondria where it decreases oxidative stress and enhances insulin secretion in response to glucose. Whether the observed increase in insulin secretion can be attributed to nuclear exclusion of pancreatic and duodenal homeobox 1, as reported previously, or whether it reflects improved processing of proinsulin to insulin and increased expression of the prohormone convertase 1/3 remains to be determined.[13,16] These insights indicate that increasing apoA-I levels may benefit hypercholesterolemic patients with impaired β-cell function.

ARTICLE INFORMATION

Received April 1, 2023; accepted November 13, 2023.

Affiliations

School of Biomedical Sciences, Faculty of Medicine (B.M., E.G., K.L.O., S.R.T., B.J.C., K.-A.R.), Katharina Gaus Light Microscopy Facility, Mark Wainwright Analytical Centre (E.P., R.M.W.), School of Biotechnology and Biomolecular Sciences (N.D., S.-Y.C., M.R.W.), and Bioanalytical Mass Spectrometry Facility, Mark Wainwright Analytical Centre (V.W.), UNSW, Sydney, Australia. ANZAC Research Institute, Concord, Sydney, Australia (M.K.).

Acknowledgments

B. Manandhar was the recipient of a University International Postgraduate Award, supported by UNSW Sydney and Commonwealth of Australia. S.-Y. Chen was supported by a UNSW Scientia PhD Scholarship.

Sources of Funding

This work was supported by the National Health and Medical Research Council of Australia (APPP2004064) to K.-A. Rye, B.J. Cochran, S.R. Thomas, R.M. Whan, and M.R. Wilkins.

Disclosures

None.

Supplemental Material

Tables S1 and S2
Figures S1–S8
Major Resources Table
Graphic abstract
Full, unedited Western Blots

REFERENCES

1. Brunham LR, Kruit JK, Pape TD, Timmins JM, Reuwer AQ, Vasanji Z, Marsh BJ, Rodrigues B, Johnson JD, Parks JS, et al. Beta-cell ABCA1 influences insulin secretion, glucose homeostasis and response to thiazolidinedione treatment. *Nat Med*. 2007;13:340–347. doi: 10.1038/nm1546
2. Hao M, Head WS, Gunawardana SC, Hasty AH, Piston DW. Direct effect of cholesterol on insulin secretion: a novel mechanism for pancreatic beta-cell dysfunction. *Diabetes*. 2007;56:2328–2338. doi: 10.2337/db07-0056
3. Ishikawa M, Iwasaki Y, Yatoh S, Kato T, Kumadaki S, Inoue N, Yamamoto T, Matsuzaka T, Nakagawa Y, Yahagi N, et al. Cholesterol accumulation and diabetes in pancreatic beta-cell-specific SREBP-2 transgenic mice: a new model for lipotoxicity. *J Lipid Res*. 2008;49:2524–2534. doi: 10.1194/jlr.M800238-JLR200
4. Kruit JK, Wijesekara N, Fox JE, Dai X-Q, Brunham LR, Searle GJ, Morgan GP, Costin AJ, Tang R, Bhattacharjee A, et al. Islet cholesterol accumulation due

to loss of ABCA1 leads to impaired exocytosis of insulin granules. *Diabetes*. 2011;60:3186–3196. doi: 10.2337/db11-0081
5. Xu Y, Toomre DK, Bogan JS, Hao M. Excess cholesterol inhibits glucose-stimulated fusion pore dynamics in insulin exocytosis. *J Cell Mol Med*. 2017;21:2950–2962. doi: 10.1111/jcmm.13207
6. Zhao YF, Wang L, Lee S, Sun Q, Tuo Y, Wang Y, Pei J, Chen C. Cholesterol induces mitochondrial dysfunction and apoptosis in mouse pancreatic beta-cell line MIN6 cells. *Endocrine*. 2010;37:76–82. doi: 10.1007/s12020-009-9275-y
7. Lu X, Liu J, Hou F, Liu Z, Cao X, Seo H, Gao B. Cholesterol induces pancreatic beta cell apoptosis through oxidative stress pathway. *Cell Stress Chaperones*. 2011;16:539–548. doi: 10.1007/s12192-011-0265-7
8. Kong FJ, Wu JH, Sun SY, Zhou JQ. The endoplasmic reticulum stress/autophagy pathway is involved in cholesterol-induced pancreatic beta-cell injury. *Sci Rep*. 2017;7:44746. doi: 10.1038/srep44746
9. Cochran BJ, Ryder WJ, Parmar A, Tang S, Reilhac A, Arthur A, Charil A, Hamze H, Barter PJ, Kritharides L, et al. In vivo PET imaging with [(18)F]FDG to explain improved glucose uptake in an apolipoprotein A-I treated mouse model of diabetes. *Diabetologia*. 2016;59:1977–1984. doi: 10.1007/s00125-016-3993-5
10. Stenkula KG, Lindahl M, Petrlova J, Dalla-Riva J, Goransson O, Cushman SW, Krupinska E, Jones HA, Lagerstedt JO. Single injections of apoA-I acutely improve in vivo glucose tolerance in insulin-resistant mice. *Diabetologia*. 2014;57:797–800. doi: 10.1007/s00125-014-3162-7
11. Du XM, Kim MJ, Hou L, Le Goff W, Chapman MJ, Van Eck M, Curtiss LK, Burnett JR, Cartland SP, Quinn CM, et al. HDL particle size is a critical determinant of ABCA1-mediated macrophage cellular cholesterol export. *Circ Res*. 2015;116:1133–1142. doi: 10.1161/CIRCRESAHA.116.305485
12. Fryirs MA, Barter PJ, Appavoo M, Tuch BE, Tabet F, Heather AK, Rye KA. Effects of high-density lipoproteins on pancreatic beta-cell insulin secretion. *Arterioscler Thromb Vasc Biol*. 2010;30:1642–1648. doi: 10.1161/ATVBAHA.110.207373
13. Cochran BJ, Bisoendial RJ, Hou L, Glaros EN, Rossy J, Thomas SR, Barter PJ, Rye KA. Apolipoprotein A-I increases insulin secretion and production from pancreatic beta-cells via a G-protein-cAMP-PKA-FoxO1-dependent mechanism. *Arterioscler Thromb Vasc Biol*. 2014;34:2261–2267. doi: 10.1161/ATVBAHA.114.304131
14. Hou L, Tang S, Wu BJ, Ong KL, Westerterp M, Barter PJ, Cochran BJ, Tabet F, Rye KA. Apolipoprotein A-I improves pancreatic beta-cell function independent of the ATP-binding cassette transporters ABCA1 and ABCG1. *FASEB J*. 2019;33:8479–8489. doi: 10.1096/fj.201802512RR
15. Cochran BJ, Hou L, Manavalan AP, Moore BM, Tabet F, Sultana A, Cuesta Torres L, Tang S, Shrestha S, Senanayake P, et al. Impact of perturbed pancreatic beta-cell cholesterol homeostasis on adipose tissue and skeletal muscle metabolism. *Diabetes*. 2016;65:3610–3620. doi: 10.2337/db16-0668
16. Nilsson O, Del Giudice R, Nagao M, Gronberg C, Eliasson L, Lagerstedt JO. Apolipoprotein A-I primes beta cells to increase glucose stimulated insulin secretion. *Biochim Biophys Acta Mol Basis Dis*. 2020;1866:165613. doi: 10.1016/j.bbadis.2019.165613
17. Miyazaki J, Araki K, Yamato E, Ikegami H, Asano T, Shibasaki Y, Oka Y, Yamamura K. Establishment of a pancreatic beta cell line that retains glucose-inducible insulin secretion: special reference to expression of glucose transporter isoforms. *Endocrinology*. 1990;127:126–132. doi: 10.1210/endo-127-1-126
18. Kritharides L, Jessup W, Gifford J, Dean RT. A method for defining the stages of low-density lipoprotein oxidation by the separation of cholesterol- and cholesteryl ester-oxidation products using HPLC. *Anal Biochem*. 1993;213:79–89. doi: 10.1006/abio.1993.1389
19. Weisweiler P. Isolation and quantitation of apolipoproteins A-I and A-II from human high-density lipoproteins by fast-protein liquid chromatography. *Clin Chim Acta*. 1987;169:249–254. doi: 10.1016/0009-8981(87)90325-1
20. Wasinger VC, Lu K, Yau YY, Nash J, Lee J, Chang J, Paramsothy S, Kaakoush NO, Mitchell HM, Leong RWL. Spp24 is associated with endocytic signalling, lipid metabolism, and discrimination of tissue integrity for 'leaky-gut' in inflammatory bowel disease. *Sci Rep*. 2020;10:12932. doi: 10.1038/s41598-020-69746-w
21. Wasinger VC, Curnoe D, Bustamante S, Mendoza R, Shoocongdej R, Adler L, Baker A, Chintakanon K, Boel C, Tacon PSC. Analysis of the preserved amino acid bias in peptide profiles of iron age teeth from a tropical environment enable sexing of individuals using amelogenin MRM. *Proteomics*. 2019;19:e1800341. doi: 10.1002/pmic.201800341
22. Patro R, Duggal G, Love MI, Irizarry RA, Kingsford C. Salmon provides fast and bias-aware quantification of transcript expression. *Nat Methods*. 2017;14:417–419. doi: 10.1038/nmeth.4197
23. Robinson MD, McCarthy DJ, Smyth GK. edgeR: a Bioconductor package for differential expression analysis of digital gene expression data. *Bioinformatics*. 2010;26:139–140. doi: 10.1093/bioinformatics/btp616
24. Risso D, Schwartz K, Sherlock G, Dudoit S. GC-content normalization for RNA-Seq data. *BMC Bioinf*. 2011;12:480. doi: 10.1186/1471-2105-12-480
25. Risso D, Ngai J, Speed TP, Dudoit S. Normalization of RNA-seq data using factor analysis of control genes or samples. *Nat Biotechnol*. 2014;32:896–902. doi: 10.1038/nbt.2931
26. Lindqvist A, Berger K, Erlanson-Albertsson C. Enterostatin up-regulates the expression of the beta-subunit of F(1)F(o)-ATPase in the plasma membrane of INS-1 cells. *Nutr Neurosci*. 2008;11:55–60. doi: 10.1179/147683008X301397
27. Das B, Mondragon MOH, Sadeghian M, Hatcher VB, Norin AJ. A novel ligand in lymphocyte-mediated cytotoxicity - expression of the beta-subunit of H+ transporting atp synthase on the surface of tumor-cell lines. *J Exp Med*. 1994;180:273–281. doi: 10.1084/jem.180.1.273
28. Moser TL, Stack MS, Asplin I, Enghild JJ, Hojrup P, Everitt L, Hubchak S, Schnaper HW, Pizzo SV. Angiostatin binds ATP synthase on the surface of human endothelial cells. *Proc Natl Acad Sci U S A*. 1999;96:2811–2816. doi: 10.1073/pnas.96.6.2811
29. Martinez LO, Jacquet S, Esteve JP, Rolland C, Cabezón E, Champagne E, Pineau T, Georgeaud V, Walker JE, Tercé F, et al. Ectopic beta-chain of ATP synthase is an apolipoprotein A-I receptor in hepatic HDL endocytosis. *Nature*. 2003;421:75–79. doi: 10.1038/nature01250
30. Carrasco-Pozo C, Tan KN, Reyes-Farias M, De La Jara N, Ngo ST, Garcia-Diaz DF, Llanos P, Cires MJ, Borges K. The deleterious effect of cholesterol and protection by quercetin on mitochondrial bioenergetics of pancreatic beta-cells, glycemic control and inflammation: in vitro and in vivo studies. *Redox Biol*. 2016;9:229–243. doi: 10.1016/j.redox.2016.08.007
31. Sakai K, Matsumoto K, Nishikawa T, Suefuji M, Nakamaru K, Hirashima Y, Kawashima J, Shirotani T, Ichinose K, Brownlee M, et al. Mitochondrial reactive oxygen species reduce insulin secretion by pancreatic beta-cells. *Biochem Biophys Res Commun*. 2003;300:216–222. doi: 10.1016/s0006-291x(02)02832-2
32. Lim S, Rashid MA, Jang M, Kim Y, Won H, Lee J, Woo J-taek, Kim YS, Murphy MP, Ali L, et al. Mitochondria-targeted antioxidants protect pancreatic beta-cells against oxidative stress and improve insulin secretion in glucotoxicity and glucolipotoxicity. *Cell Physiol Biochem*. 2011;28:873–886. doi: 10.1159/000335802
33. Cavelier C, Ohnsorg PM, Rohrer L, von Eckardstein A. The beta-chain of cell surface F(0)F(1) ATPase modulates apoA-I and HDL transcytosis through aortic endothelial cells. *Arterioscler Thromb Vasc Biol*. 2012;32:131–139. doi: 10.1161/ATVBAHA.111.238063
34. Huang Q, Merriman C, Zhang H, Fu D. Coupling of insulin secretion and display of a granule-resident zinc transporter ZnT8 on the surface of pancreatic beta cells. *J Biol Chem*. 2017;292:4034–4043. doi: 10.1074/jbc.M116.772152
35. Taurino F, Gnoni A. Systematic review of plasma-membrane ecto-ATP synthase: a new player in health and disease. *Exp Mol Pathol*. 2018;104:59–70. doi: 10.1016/j.yexmp.2017.12.006
36. Radojkovic C, Genoux A, Pons V, Combes G, de Jonge H, Champagne E, Rolland C, Perret B, Collet X, Tercé F, et al. Stimulation of cell surface F1-ATPase activity by apolipoprotein A-I inhibits endothelial cell apoptosis and promotes proliferation. *Arterioscler Thromb Vasc Biol*. 2009;29:1125–1130. doi: 10.1161/ATVBAHA.109.187997
37. Rohrer L, Cavelier C, Fuchs S, Schluter MA, Volker W, von Eckardstein A. Binding, internalization and transport of apolipoprotein A-I by vascular endothelial cells. *Biochim Biophys Acta*. 2006;1761:186–194. doi: 10.1016/j.bbalip.2006.01.009
38. Schmidt C, Lepsverdize E, Chi SL, Das AM, Pizzo SV, Dityatev A, Schachner M. Amyloid precursor protein and amyloid beta-peptide bind to ATP synthase and regulate its activity at the surface of neural cells. *Mol Psychiatry*. 2008;13:953–969. doi: 10.1038/sj.mp.4002077
39. Neuspiel M, Schauss AC, Braschi E, Zunino R, Rippstein P, Rachubinski RA, Andrade-Navarro MA, McBride HM. Cargo-selected transport from the mitochondria to peroxisomes is mediated by vesicular carriers. *Curr Biol*. 2008;18:102–108. doi: 10.1016/j.cub.2007.12.038
40. Soubannier V, McLelland GL, Zunino R, Braschi E, Rippstein P, Fon EA, McBride HM. A vesicular transport pathway shuttles cargo from mitochondria to lysosomes. *Curr Biol*. 2012;22:135–141. doi: 10.1016/j.cub.2011.11.057
41. Zhou AL, Swaminathan SK, Curran GL, Poduslo JF, Lowe VJ, Li L, Kandimalla KK. Apolipoprotein A-I crosses the blood-brain barrier through clathrin-independent and cholesterol-mediated endocytosis. *J Pharmacol Exp Ther*. 2019;369:481–488. doi: 10.1124/jpet.118.254201

42. Wang T, Chen Z, Wang X, Shyy JY, Zhu Y. Cholesterol loading increases the translocation of ATP synthase beta chain into membrane caveolae in vascular endothelial cells. *Biochim Biophys Acta*. 2006;1761:1182–1190. doi: 10.1016/j.bbalip.2006.08.009
43. Lorenzo PI, Fuente-Martin E, Brun T, Cobo-Vuilleumier N, Jimenez-Moreno CM, G Herrera Gomez I, López Noriega L, Mellado-Gil JM, Martin-Montalvo A, Soria B, et al. PAX4 Defines an expandable beta-cell subpopulation in the adult pancreatic islet. *Sci Rep*. 2015;5:15672. doi: 10.1038/srep15672
44. Segerstolpe A, Palasantza A, Eliasson P, Andersson E-M, Andréasson A-C, Sun X, Picelli S, Sabirsh A, Clausen M, Bjursell MK, et al. Single-cell transcriptome profiling of human pancreatic islets in health and type 2 diabetes. *Cell Metab*. 2016;24:593–607. doi: 10.1016/j.cmet.2016.08.020
45. Dorrell C, Schug J, Canaday PS, Russ HA, Tarlow BD, Grompe MT, Horton T, Hebrok M, Streeter PR, Kaestner KH, et al. Human islets contain four distinct subtypes of beta cells. *Nat Commun*. 2016;7:11756. doi: 10.1038/ncomms11756
46. Rohrl C, Eigner K, Winter K, Korbelius M, Obrowsky S, Kratky D, Kovacs WJ, Stangl H. Endoplasmic reticulum stress impairs cholesterol efflux and synthesis in hepatic cells. *J Lipid Res*. 2014;55:94–103. doi: 10.1194/jlr.M043299
47. Johnson JD, Kuang S, Misler S, Polonsky KS. Ryanodine receptors in human pancreatic beta cells: localization and effects on insulin secretion. *FASEB J*. 2004;18:878–880. doi: 10.1096/fj.03-1280fje
48. Liu M, Weiss MA, Arunagiri A, Yong J, Rege N, Sun J, Haataja L, Kaufman RJ, Arvan P. Biosynthesis, structure, and folding of the insulin precursor protein. *Diabetes Obes Metab*. 2018;20(Suppl 2):28–50. doi: 10.1111/dom.13378
49. Gorlach A, Klappa P, Kietzmann T. The endoplasmic reticulum: folding, calcium homeostasis, signaling, and redox control. *Antioxid Redox Signal*. 2006;8:1391–1418. doi: 10.1089/ars.2006.8.1391
50. Baron M, Veres A, Wolock SL, Faust AL, Gaujoux R, Vetere A, Ryu JH, Wagner BK, Shen-Orr SS, Klein AM, et al. A single-cell transcriptomic map of the human and mouse pancreas reveals inter- and intra-cell population structure. *Cell Syst*. 2016;3:346–360.e4. doi: 10.1016/j.cels.2016.08.011
51. Xin Y, Dominguez Gutierrez G, Okamoto H, Kim J, Lee A-H, Adler C, Ni M, Yancopoulos GD, Murphy AJ, Gromada J. Pseudotime ordering of single human beta-cells reveals states of insulin production and unfolded protein response. *Diabetes*. 2018;67:1783–1794. doi: 10.2337/db18-0365
52. Johnston NR, Mitchell RK, Haythorne E, Pessoa MP, Semplici F, Ferrer J, Piemonti L, Marchetti P, Bugliani M, Bosco D, et al. Beta cell hubs dictate pancreatic islet responses to glucose. *Cell Metab*. 2016;24:389–401. doi: 10.1016/j.cmet.2016.06.020
53. Garner B, Waldeck AR, Witting PK, Rye KA, Stocker R. Oxidation of high density lipoproteins. II. Evidence for direct reduction of lipid hydroperoxides by methionine residues of apolipoproteins AI and AII. *J Biol Chem*. 1998;273:6088–6095. doi: 10.1074/jbc.273.11.6088
54. Barter PJ, Nicholls S, Rye KA, Anantharamaiah GM, Navab M, Fogelman AM. Antiinflammatory properties of HDL. *Circ Res*. 2004;95:764–772. doi: 10.1161/01.RES.0000146094.59640.13
55. Jo S, Beetch M, Gustafson E, Wong A, Oribamise E, Chung G, Vadrevu S, Satin LS, Bernal-Mizrachi E, Alejandro EU. Sex differences in pancreatic β-cell physiology and glucose homeostasis in C57BL/6J mice. *J Endocr Soc*. 2023;7:bvad099. doi: 10.1210/jendso/bvad099